JACS Au
AN OPEN ACCESS JOURNAL OF THE AMERICAN CHEMICAL SOCIETY

pubs.acs.org/jacsau
Perspective

Design of Supported Metal Catalysts and Systems for Propane Dehydrogenation

Zhe He, Jingnan Yang, and Lichen Liu*

Cite This: *JACS Au* 2024, 4, 4084−4109
Read Online

ABSTRACT: Propane dehydrogenation (PDH) is currently an approach for the production of propylene with high industrial importance, especially in the context of the shale gas revolution and the growing global demands for propylene and downstream commodity chemicals. In this Perspective article, we comprehensively summarize the recent advances in the design of advanced catalysts for PDH and the new understanding of the structure−performance relationship in supported metal catalysts. Furthermore, we discuss the gaps between fundamental research and practical industrial applications in the catalyst developments for the PDH process. In particular, we overview some critical issues regarding catalyst regeneration and the compatibility of the catalyst and reactor design. Finally, we make perspectives on the future directions of PDH research, including the efforts toward achieving a unified understanding of the structure−performance relationship, innovation in reactor engineering, and translation of the knowledge accumulated on PDH studies to other important alkane dehydrogenation reactions.

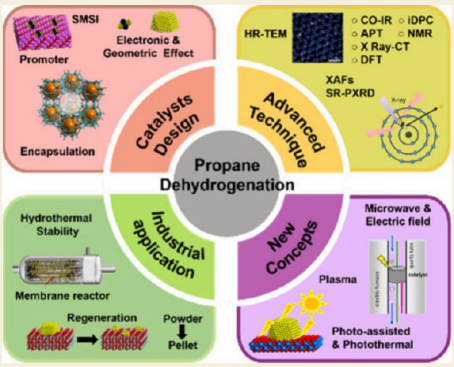

KEYWORDS: *Propane dehydrogenation, platinum, alumina, alloy, metal clusters, zeolite, membrane reactor, catalyst deactivation, catalyst regeneration*

1. INTRODUCTION

Propylene, a pivotal commodity chemical for producing high-value chemicals such as polypropylene, epichlorohydrin, acrylonitrile, and acetone, is witnessing a ∼5% growth rate of annual global demand.[1−4] Among the diverse technologies for propylene production, propane dehydrogenation (PDH) stands out for its conversion efficiency, atomic utilization, and high selectivity compared to traditional processes such as steam cracking (SC) and fluid catalytic cracking (FCC).[5−7] Moreover, the discovery of abundant shale gas resources in North America has led to a significant drop in propane prices, while oil prices have surged during the last two decades, resulting in sharply increased interest in PDH from industry and academia.[8]

However, due to thermodynamic limitations, direct non-oxidative propane dehydrogenation (DPDH) reactions typically require elevated temperatures (>550 °C), resulting in coke-induced catalyst deactivation.[9] Although oxidative propane dehydrogenation (OPDH) can mitigate carbon formation, it suffers from a declined selectivity to propylene and complex gas constituents that elevate the separation costs.[6,10,11] Therefore, adopting DPDH processes is crucial for effective propylene production, as demonstrated in commercial applications such as the Catofin process based on CrO_x/Al_2O_3 catalysts and the Oleflex process based on $PtSn/Al_2O_3$ catalysts.[4] Despite their applications in numerous plants, these commercial techniques encounter several operational challenges. For instance, the frequent oxidative regenerations of $PtSn/Al_2O_3$ are required to remove the carbon deposition, which may cause the sintering of Pt active sites and restrict the catalyst's reusability. Moreover, despite the lower fabrication costs of CrO_x/Al_2O_3 catalysts, they exhibit intrinsically lower activity and inferior propylene selectivity than Pt-based catalysts, while containing toxic Cr components with potential health and environmental issues.[1,7]

As illustrated in Figure 1, researchers are addressing these challenges through two major methods: 1) optimizing the catalyst supports, such as Al_2O_3, SiO_2, TiO_2, CeO_2, carbon materials, mesoporous materials, and zeolites; and 2) incorporating metal functional components such as Pt, Pd, Rh, Ni, Fe, Co, Zn, Cr, V, and Ga.[12−25] Although these catalysts demonstrate excellent performance at the laboratory scale in comparison to the conventional Al_2O_3-supported metal catalysts, the durability of the sophisticatedly designed active sites under rigorous industrial conditions requires further validation, and the catalyst deactivation after multiple oxidative−reductive regenerations remains a challenge. Though

Received: August 11, 2024
Revised: October 18, 2024
Accepted: October 22, 2024
Published: October 29, 2024

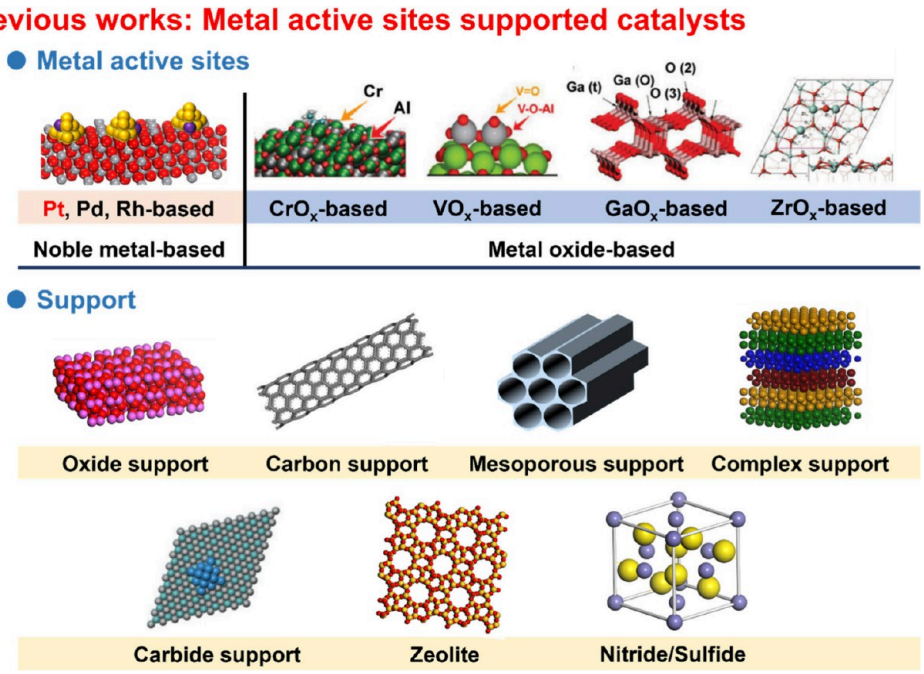

Figure 1. Schematic illustrations of supported metal catalysts for PDH. The supported metal catalysts consist of two major components: the metal active sites and the solid carriers. In this figure, we have listed the typical materials for the construction of PDH catalysts. Reproduced with permission from ref 2. Copyright 2021 Royal Society of Chemistry.

some of the bulk oxide catalysts are reported as active catalysts for PDH, the space-time yields of propylene are still considerably lower than the conventional supported Pt, CrO_x and GaO_x catalysts.[26,27]

Herein, we review the contemporary strategies to enhance the conversion efficiency and stability of PDH catalysts and discuss the latest progress in the design of advanced PDH catalysts based on active sites with novel structural features. In particular, we will emphasize the atomic insights into the active sites and their structure-performance relationship. Furthermore, we will highlight the emerging concepts of the PDH process, such as membrane reactors and electric field-assisted dehydrogenation that hold promise for overcoming current limitations and further advancing the field of propylene production.

2. RECENT ADVANCES IN THE DEVELOPMENT OF PDH CATALYSTS

2.1. PDH Catalysts Based on Noble Metals

Pt-based catalysts are considered most effective for PDH reactions due to their high preference for C−H bond activation over the C−C bond cleavage. While monometallic Pt catalysts exhibit strong C−H bond activation, this particular strength leads to rapid deactivation through extensive dehydrogenation and subsequent carbon accumulation.[4] Introducing a secondary metal is one of the most efficient strategies for optimizing the properties of the active sites and mitigating catalyst deactivation.

As illustrated in Figure 2a−b, the beneficial effects of the secondary metal are derived from two aspects: electronic effect and geometric effect.[2,28−34] Specifically, the introduction of a secondary metal enhances the electron density of Pt atoms through interatomic electron transfer, which in turn broadens the d-band and consequently lowers the d-band center at Pt active sites. This modification facilitates the desorption of C_3H_6 and the transfer of coke from the Pt sites to the support. Simultaneously, the incorporation of the secondary metal, acting through a dilution effect, breaks down larger Pt nanoparticles into smaller clusters, effectively eliminating the active sites that are prone to coke formation.

Various metals, including Sn, Ga, In, Zn, Fe, Cu, and Co, have been utilized as promoters in Pt-based alkane dehydrogenation catalysts, with Sn being the most commonly used additive. While the PtSn catalyst has been commercially applied for decades in the Oleflex process for PDH, research efforts are continuously dedicated to enhancing its stability and specific activity of the Pt sites. For instance, by premixing H_2PtCl_6 and $SnCl_2$ solutions before impregnation to create a Pt−Sn bimetallic coordination complex, the obtained $PtSn/SiO_2$ catalyst can sustain PDH reactions at conversion levels near thermodynamic equilibrium with a 99% C_3H_6 selectivity. The key to the exceptional performance lies in maintaining a close proximation between Pt and Sn species in the intermetallic PtSn nanoparticles confirmed by various electron microscopy and spectroscopy characterizations (Figure 2c−e).[35]

Similar to Pt-based catalysts, Rh-based catalysts also demonstrate notable C−H bond activation capabilities, though they are less explored due to the high prices of Rh. Additionally, their capability to activate C−C bonds often promotes undesired C−C cracking and coke deposition.[21,36−38] Similar as the Pt-based catalysts, a secondary metal is also introduced into Rh to form bimetallic active sites to suppress the undesired side reactions. For example, a RhIn@MFI catalyst derived from one-pot synthesis exhibits exceptional stability for up to 5500 h when using pure C_3H_8 as the feed. The stability is attributed to the formation of bimetallic RhIn particles within the pure-silica MFI zeolite matrix (Figure 2f−i).[39] The Rh atoms in the RhIn bimetallic particles are separated by the In atoms, leading to the formation of single-atom sites, which greatly suppress the coke deposition on Rh.

Notably, based on reported large-scale catalyst preparation methods, an excessive amount of the secondary metal is typically

https://doi.org/10.1021/jacsau.4c00730
JACS Au 2024, 4, 4084−4109

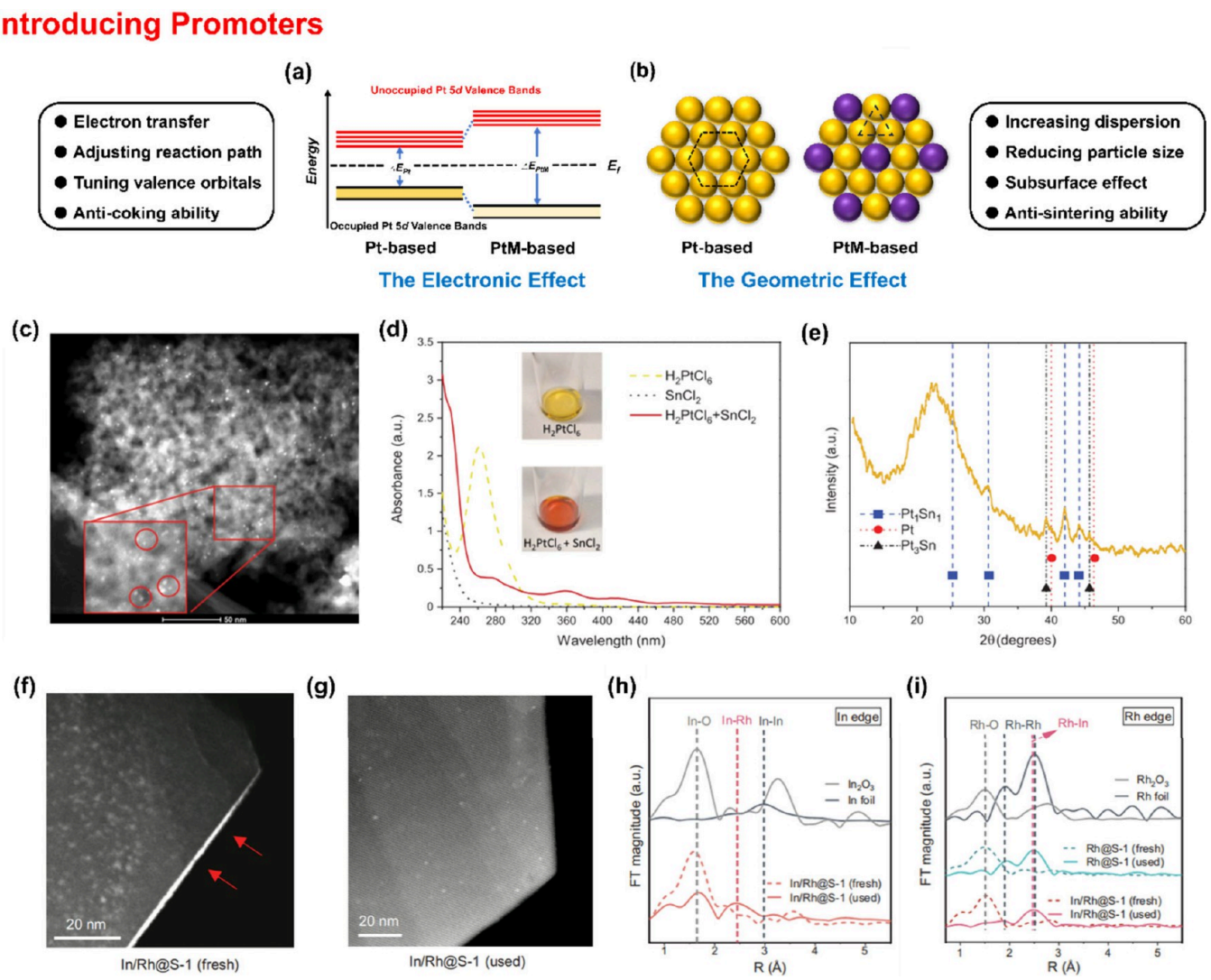

Figure 2. Illustrations of secondary metal species promoting effects on Pt-based catalysts. (a) Modifying the electronic structures of Pt active sites by forming bimetallic PtM particles. (b) Modifying the geometric structures of Pt active sites by controlling the ensemble size of Pt atoms. (c) A STEM image of PtSn alloy nanoparticles supported on silica. (d) UV−vis absorption spectra of Pt−Sn bimetallic precursor solutions. Changes in the absorption peaks and color of the liquid suggest the formation of Pt−Sn complexes. (e) X-ray diffraction pattern of $PtSn/SiO_2$, indicating the formation of PtSn and Pt_3Sn alloys. Reproduced with permission from ref 35. Copyright 2021 American Association for the Advancement of Science. The HADDF-STEM images of (f) In/Rh@S-1-fresh and (g) In/Rh@S-1 -used. k^2-weighted EXAFS spectra at the (h) In K-edge and (i) Rh K-edge for In/Rh@S-1 and reference samples. The HADDF-STEM images show the metal migration process in the reducing atmosphere, and the EXAFS results show the formation of Rh−In bonds, proving that Rh and In species are approximately close. Reproduced with permission from ref 39. Copyright 2024 American Association for the Advancement of Science.

required to ensure sufficient contact with Pt or Rh. This may lead to the formation of large particles of secondary metal oxides (MO_x), triggering side reactions such as cracking and carbon formation. Furthermore, after multiple cycles of oxidation to remove carbon and subsequent reduction, the secondary metal in the Pt/Rh-based bimetallic particles segregates and aggregates into MO_x particles, leading to irreversible deformation of the optimal active sites.[1,7,40] As highlighted in the above discussions, the formation of bimetallic active sites with high uniformity and structural robustness remains a challenge in the preparation of supported metal catalysts for PDH. Recently, it has been proposed that high-entropy Pt-based alloys exhibit higher stability against segregation than conventional bimetallic systems during reduction−oxidation treatments, which could be ascribed to the interaction between Pt and the surrounding atoms.[41] For instance, the reported high-entropy intermetallic compound $(PtCoCu)(GeGaSn)/Ca\text{-}SiO_2$ catalyst demonstrates significantly enhanced catalytic stability and selectivity compared to the PtGe catalyst and exhibits a very long catalyst lifetime up to 4146 h. The advanced characterizations and model calculations reveal that site-isolation and entropy effects significantly improve the desorption and thermal stability of C_3H_6 on the high-entropy alloyed catalyst, enabling superior performance even in high-temperature reaction environments.[42] The advantage of high-entropy alloys is also reflected in CO_2-assisted PDH.[43] However, a fundamental issue related to Pt-based high-entropy alloy catalysts is identifying the optimal active site for PDH because the propane molecule can only interact with a few atoms (probably less than 5) during the catalytic cycle.

In recent years, Pt single-atom alloy catalysts constructed by introducing a second metal as the host have also demonstrated

https://doi.org/10.1021/jacsau.4c00730
JACS Au 2024, 4, 4084−4109

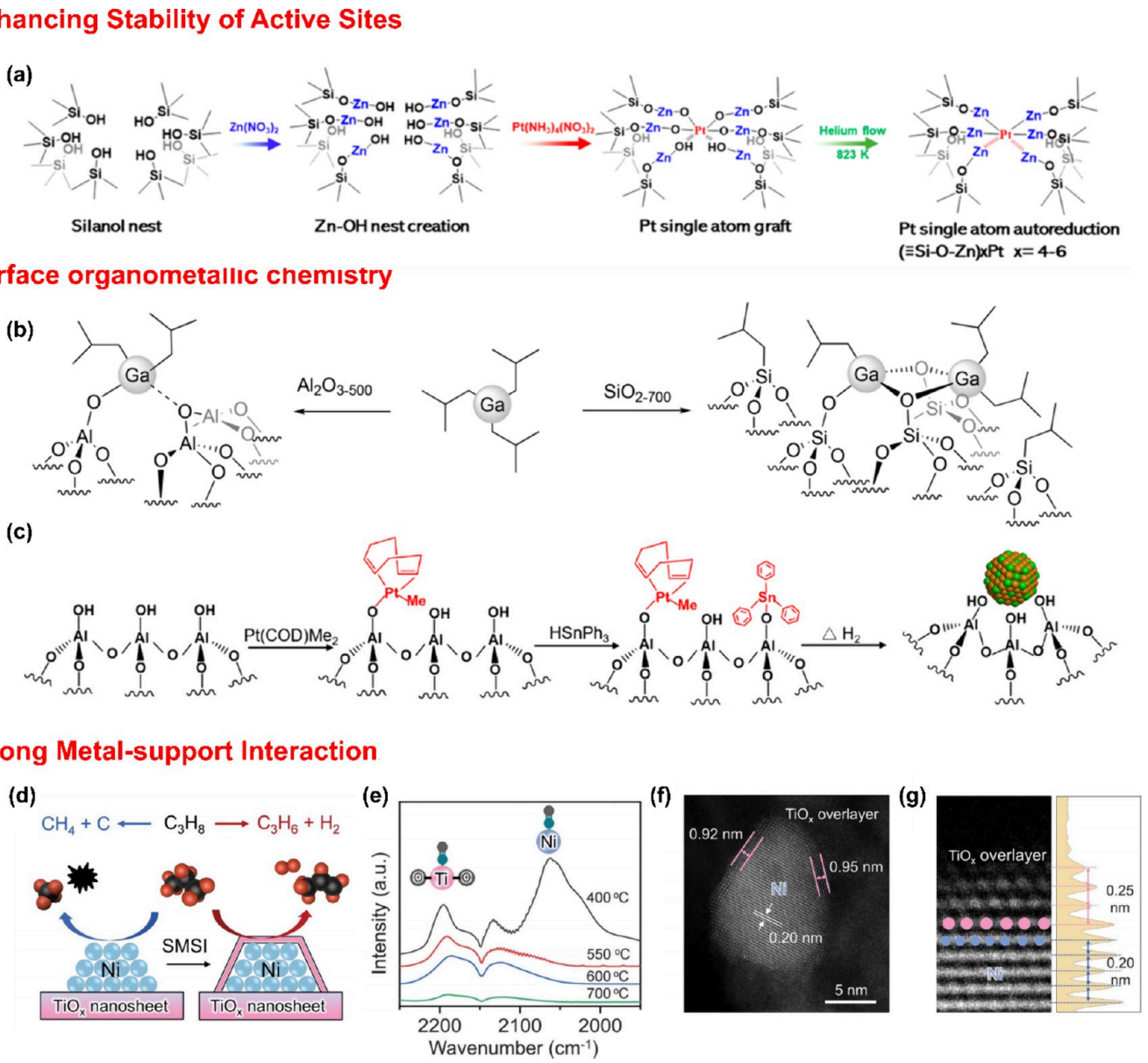

Figure 3. Schematic illustrations of synthesis methods for specific catalyst structures. (a) The $(\equiv Si{-}O{-}Zn)_{4-6}Pt$ structure stabilized by Si−O−Zn−OH sites in dealuminated Beta zeolite. Reproduced with permission from ref 59. Copyright 2021 American Chemical Society. (b) The mononuclear and binuclear surface Ga species formed by grafting $Ga(i\text{-}Bu)_3$ onto Al_2O_3 and SiO_2. Reproduced with permission from ref 62. Copyright 2018 American Chemical Society. (c) The preparation of PtSn species through the grafting of $Pt(COD)Me_2$ and Ph_3SnH onto dehydroxylated Al_2O_3. (d) Schematic illustration of the Ni@TiO_x structures for PDH. Reproduced with permission from ref 63. Copyright 2019 Elsevier. (e) CO-IR spectra of the Ni-TiO_2/Al_2O_3 catalysts obtained after different reduction treatments, highlighting the absence of CO adsorption bands on Ni particles, which suggests encapsulation by oxide overlayers. (f, g) Atomic structures of the Ni@TiO_x structures arising from strong metal−support interactions. Reproduced with permission from ref 64. Copyright 2024 American Association for the Advancement of Science.

excellent catalytic performance in PDH processes.[44] For instance, a Pt/Cu single-atom alloy supported on Al_2O_3 prepared through coimpregnation and atomic dilution strategies showed catalytic effects markedly different from traditional alloy catalysts.[45] In both Pt/Cu single-atom alloy and traditional alloy surfaces, the activation mode of the C−H bond in propane just involves a single adsorption configuration at the Pt−Cu sites, leading to similar dehydrogenation activities. However, in traditional alloys catalysts, a propene molecule can interact simultaneously with three Pt atoms and stabilize at a triple-vacancy site, exhibiting a lower deep dehydrogenation barrier (<1 eV). In contrast, on the surface of the Pt/Cu single-atom alloy, C_3H_5 (a precursor model for carbon formation) interacts only with a single Pt atom, resulting in a higher deep dehydrogenation barrier (>2 eV), thereby achieving high selectivity and activity in PDH reactions. However, with copper as the host in the single-atom alloy, its lower Tamman temperature (about 405 °C) makes it prone to sintering and aggregation at high temperatures (above 550 °C), leading to rapid deactivation of the catalyst. To address this issue, the authors optimized the support and loading methods by using a steam-ammonia hydrothermal process to first combine copper with silica, creating a copper silicate precursor support. Subsequently, by impregnating trace amounts of Pt, a stable PtCu single-atom alloy catalyst precursor was successfully prepared.[46] This step effectively suppressed the growth of

https://doi.org/10.1021/jacsau.4c00730
JACS Au 2024, 4, 4084−4109

alloy particles with rising temperature, thus enhancing the catalyst's stability.

2.2. PDH Catalysts Based on Non-noble Metals

Besides the catalysts based on noble metals, researchers are also interested in supported metal oxide catalysts because of their low prices, such as CoO_x, ZnO_x, VO_x, and CrO_x.[4,47] Unlike the mechanism of Pt/Rh-based catalysts that directly activate the C−H bond on the metallic sites, metal oxide catalysts rely on their highly dispersed M-O sites for C−H bond activation. Introducing metal oxide additives into the oxide-based catalysts can alter their coordination environment and/or electronic states, thereby enhancing the activity and stability of the catalysts. For example, by incorporating CrO_x into ZrO_x/SiO_2, the $CrZrO_x/SiO_2$ catalyst demonstrates excellent catalytic stability after 50 dehydrogenation and regeneration cycles without a significant decrease in activity.[48] In comparison to the catalysts based on noble metals, the oxide catalysts exhibit much higher stability during reaction-regeneration cycles due to the strong M-O bonding with the support. In particular, by incorporating the non-noble metal sites into the zeolite structure, their specific activity and stability will be further promoted in comparison to those supported on alumina or silica. For instance, a variety of non-noble metal species (e.g., Zn, Ga, In, Co, Mo, etc.) are introduced to MFI-, *BEA- and CHA-type zeolites as extra-framework active sites for PDH.[49] Though these materials have been extensively studied by numerous techniques and many different research groups, there are still some arguments on the structural features of the active sites, as reflected in the zeolite-supported Ga catalysts.[50−52] According to recent studies, it is confirmed that the catalytic properties of non-noble metal active sites can be greatly affected by the ensemble size (atomicity of the non-noble metal species), chemical states and the zeolite scaffold surrounding the metal species.[53,54]

However, it should be noted that the specific activities of supported metal oxide-based catalysts are much lower than the Pt/Rh-based catalysts, which require the use of a higher number of solid catalysts for achieving similar productivity as the noble metal catalysts. One strategy to improve the activity of oxide catalysts is to introduce trace amounts of noble metals, resulting in metal-oxide bimetallic catalysts for PDH. In the example of GaO_x/Al_2O_3, adding 1000 ppm of Pt can significantly enhance the catalytic activity, which is attributed to the promoted formation of $Ga^{\delta+}$−H species on GaO_x particles, which are proposed as the active sites for C−H activation.[55,56] From a fundamental point of view, it is interesting to study the appropriate ensemble size of the Pt on the GaO_x particles.

2.3. Control of the Metal−Support Interface

The selection of solid carriers for the active sites is vital for achieving high activity in PDH, as the metal−support interaction can effectively tune the activity and stability of the metal species.[57,58] Normally, oxides are selected as the solid carriers because of the strong interaction between the metal active sites and the oxide carriers. Moreover, oxide carriers have much higher stability in consecutive exposure to oxidative and reduction atmospheres during the reaction-regeneration cycles than other materials such as porous carbon, nitride/sulfide. Moreover, oxide supports with microporous features are more desired over open-structure carriers because the metal active sites can be accommodated in the micropores for improvement in thermal stability. For example, impregnating Zn onto dealuminated Beta zeolite can effectively stabilize Pt with the Si−O−Zn−OH sites, and the resulting bimetallic PtZn sites exhibit superior stability and PDH activity (Figure 3a). With cofeeding H_2, the catalyst maintains the activity after four reaction-regeneration cycles.[59] This method is also applicable in the synthesis of bimetallic PtZn sites supported on self-pillared zeolite pentasil nanosheets for PDH and butane dehydrogenation reactions.[60] In a similar vein, a high-performance Zn_1Co_1−N−C heteronuclear dual-atom catalyst has been developed, where the N-bridged Zn_1Co_1 dual atom pair serves as the primary active center for the PDH reaction.[61] Strong covalent bonds between the N species and metal M stabilize the metal in a specific valence state, enhancing its stability and effectively suppressing the reduction and volatilization of Zn. Compared to Zn_1/NC, Co_1/NC monatomic catalysts, and Zn_2/NC diatomic catalysts, the Zn_1Co_1 catalyst exhibits higher activity and selectivity. This is due to the electronic interactions between Zn_1 and Co_1 coordinated by the N species, which promote the activation of the C−H bonds in C_3H_8. During the reaction, the generated H species covers the Zn_1 position, further promoting the desorption of propylene from the Co_1 site, thereby enhancing selectivity. The prepared catalyst performs comparably to industrial CrO_x-based catalysts in terms of reactivity and exhibits greater stability.

The metal−supports interaction can be significantly enhanced by employing the surface organometallic chemistry (SOMC) method, which involves the formation of strong covalent M−O bonds between the organometallic precursor and the oxide support. The presence of −OH groups on the high-surface-area solid carriers serves as the anchoring sites for the organometallic precursors. For instance, by grafting $Ga(i\text{-}Bu)_3$ (where i-Bu = $CH_2CH\text{-}(CH_3)_2$) onto Al_2O_3 or SiO_2 surfaces, mononuclear $[(\text{-}AlO)Ga(i\text{-}Bu)_2O]$ and binuclear $[(\text{-}SiO)_2Ga_2(i\text{-}Bu)_3]$ sites are generated, respectively (Figure 3b). The mononuclear Ga sites on Al_2O_3 display significantly higher activity than the binuclear sites on SiO_2, possibly due to the higher C−H bond activation ability.[62]

Furthermore, the SOMC method can precisely adjust bimetallic sites at the atomic level. As illustrated in Figure 3c, by sequentially loading dimethyl(1,5-cyclooctadiene)platinum-(II) ($Pt(COD)Me_2$) and triphenyltin hydride (Ph_3SnH) onto dehydroxylated Al_2O_3, $[\equiv AlO\text{-}Pt(COD)Me]$ and $[\equiv AlO\text{-}SnPh_3]$ sites are successfully immobilized on Al_2O_3 surface. The subsequent hydrogenolysis under mild conditions leads to the formation of bimetallic Pt−Sn clusters (<0.75 nm). Notably, the unique $Pt\text{−}Sn/Al_2O_3$ catalysts exhibit significantly higher PDH catalytic activity and stability than catalysts prepared by traditional impregnation methods because the conventional method cannot ensure intimate Pt−Sn contact.[63] Despite the precise control of active sites through the SOMC method, the high price of organometallic precursors restricts its practical application in commercial process.

Current research on SMSI primarily focuses on optimizing the performance of traditional PDH active metal elements (such as Pt, Ga, Zn, Co, Ni, etc.), while oxide support materials are generally seen only as promoters instead of the main active sites for PDH. In a recent study, as illustrated in Figure 3d−g, a $Ni\text{-}TiO_2/Al_2O_3$ catalyst demonstrated marked PDH activity and stability (>150 h), in which the defective TiO_x layers covered on Ni nanoparticles act as the primary active site for PDH. The Ti^{3+} species, identified as the active sites and formed at tetracoordinated Ti_{4C} sites with oxygen vacancies, were detected within the defective TiO_x overlayers, which are formed due to the strong-metal support interaction induced by high-temper-

https://doi.org/10.1021/jacsau.4c00730
JACS Au 2024, 4, 4084−4109

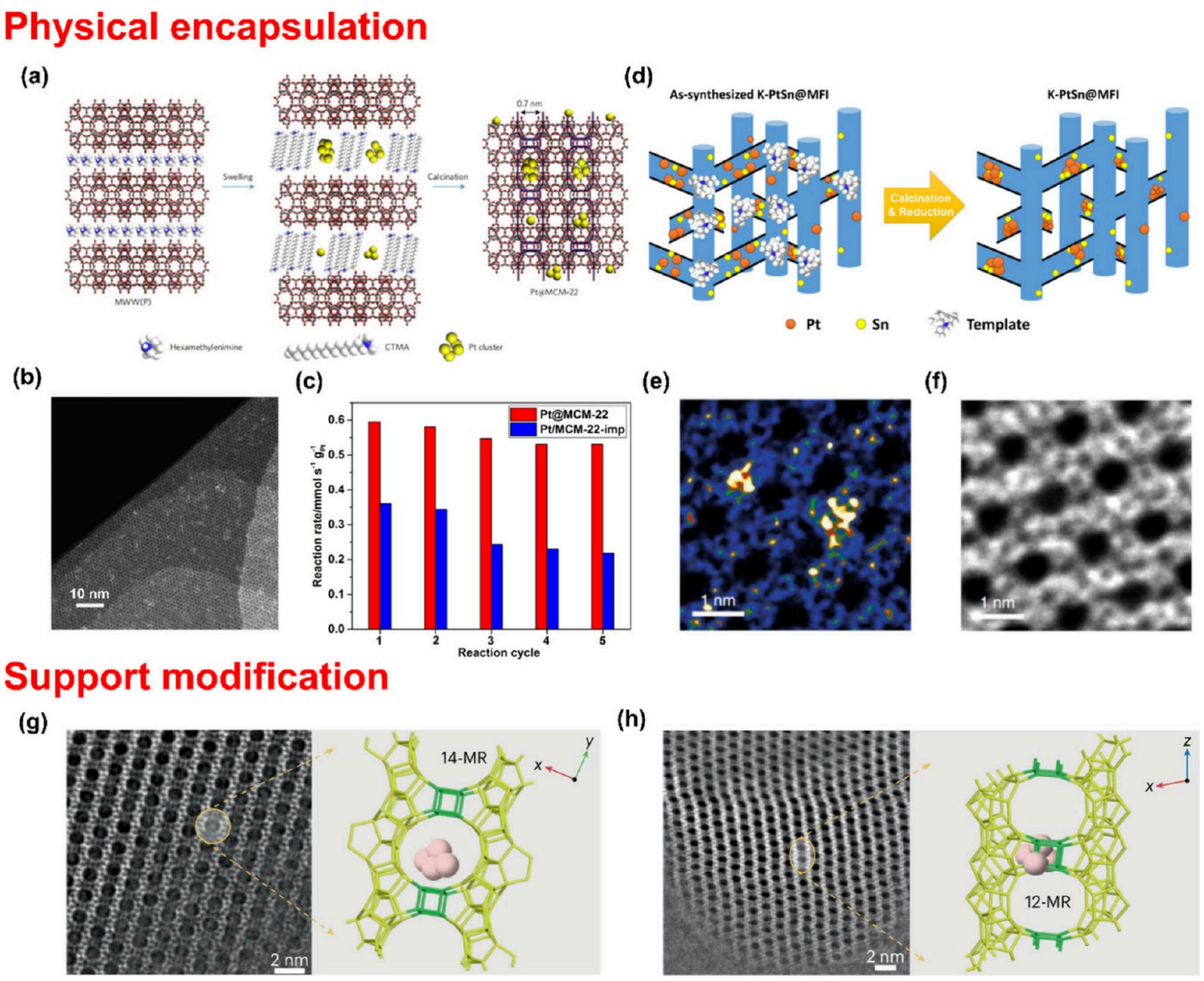

Figure 4. Zeolite-supported metal catalysts for PDH. (a) Illustration of the formation mechanism of Pt@MCM-22 catalysts through a transformation of a two-dimensional zeolite into three-dimensional structure. (b) The HR-HAADF-STEM image of Pt@MCM-22, showing the presence of single Pt atoms and Pt clusters encapsulated in pure-silica MCM-22. (c) PDH test for Pt@MCM-22 and Pt/MCM-22-imp catalysts over five reaction-regeneration cycles at 550 °C. Reproduced with permission from ref 65. Copyright 2017 Spring Nature. (d) Schematic illustration of the formation mechanism of K-PtSn@MFI catalysts synthesized by one-post synthesis. (e, f) The HR HAADF-STEM and iDPC images of the K-PtSn@MFI catalysts in the [010] direction. After reduction with H_2, subnanometer metal clusters are encapsulated in the sinusoidal 10MR channels of MFI zeolite. Reproduced with permission from ref 66. Copyright 2019 Spring Nature. (g, h) iDPC-STEM images of Pt/Ge-UTL catalyst in the [001] and [010] direction, showing the formation of tiny Pt clusters within UTL-type zeolite. Reproduced with permission from ref 76. Copyright 2023 Spring Nature.

ature reduction treatment. Further analysis of the electronic interactions between the Ni nanoparticles and the TiO_x overlayers reveals electron accumulation at the interfacial Ni atoms, creating electron-rich Ni sites.[64]

Despite the excellent activity demonstrated by the aforementioned catalysts, most supported catalysts currently focus on strengthening metal−support interface suffer from a common issue: their complex preparation methods often require cumbersome processes and expensive chemicals, leading to low economic efficiency. A preparation method for ZnO-supported catalysts has been proposed to address this issue. In this method, metal oxides and carriers (such as zeolites or common metal oxides) are used either as physical mixtures or in a bilayer arrangement (with ZnO positioned in the upper layer). After reduction treatment above 550 °C, the OH groups on the carrier react with Zn atoms, forming active ZnO_x species in situ. Subsequently, under the same apparatus and industrial-related conditions, the ZnO-S-1 catalyst showed a three times higher propylene yield than the commercial K-CrO_x/Al_2O_3 catalyst. Additionally, this method has proven effective for preparing other active zinc-containing catalysts, such as using different silica-based zeolites (like dealuminated zeolite, Beta, and MCM-22), or commercially available OH-rich metal oxides (such as Al_2O_3, TiO_2, $LaZrO_x$, $TiZrO_x$, and ZrO_2−SiO_2) in either physical mixtures or bilayer forms, all exhibiting excellent activity.[16] Although finding an active metal precursor that can migrate in a reducing (or even oxidizing) atmosphere may be a limitation of this technology, it is undeniable that this method of catalyst preparation offers new insights for PDH catalysts, and expanding this technology to other metals and carrier systems is expected to inject new life into PDH technology.

2.4. Confining the Active Sites in Porous Support

When the noble metals are supported on an open-structure surface, their sintering under harsh PDH reaction conditions is inevitable. In recent years, a series of studies have shown that

https://doi.org/10.1021/jacsau.4c00730
JACS Au 2024, 4, 4084−4109

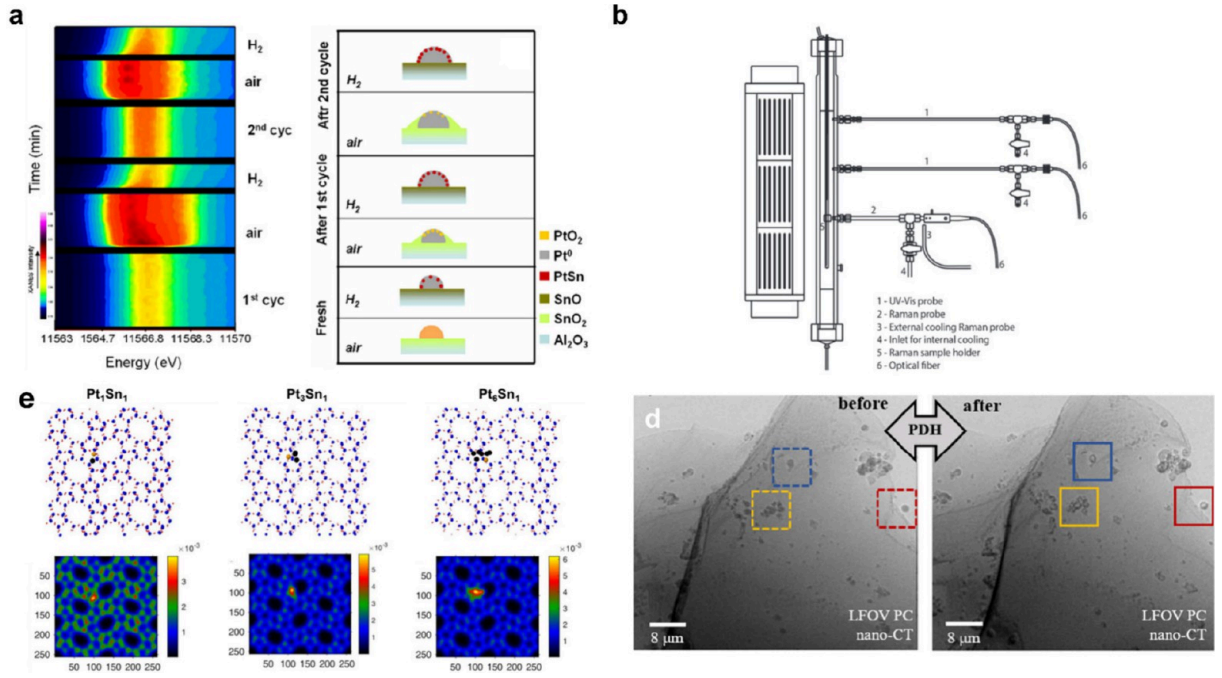

Figure 5. Advanced characterizations used for PDH catalysts. (a) Intensity contour map of the HERFD XANES spectra of the Pt−Sn/Al_2O_3 catalyst acquired at 600 °C during the first two propane dehydrogenation−regeneration cycles and the corresponding illustration. Reproduced with permission from ref 40. Copyright 2010 Elsevier (b) Detailed scheme of the pilot-scale reactor for investigating the deactivation of CrO_x/Al_2O_3 extrudates during PDH. Reproduced with permission from ref 79. Copyright 2014 European Chemical Society. (c) HAADF-STEM simulations of Pt_1Sn_1, Pt_3Sn_1, and Pt_6Sn_1 species encapsulated within pure-silica MFI zeolite, based on models derived from DFT calculations. Reproduced with permission from ref 68. Copyright 2024 American Chemical Society. (d) Single projected images of a porous SiO_2 bead loaded with Ga−Pt SCALMS primary particles before and after PDH. Reproduced with permission from ref 88. Copyright 2024 American Chemical Society.

incorporating the metal active sites into microporous supports can greatly promote the stability of the noble metals by imposing confinement effects on the active sites. Taking metal@zeolite catalysts as an example, subnanometer Pt clusters are successfully encapsulated within the interlayer space of MCM-22 zeolite, using hexadecyltrimethylammonium as a surfactant and dimethylformamide as a capping agent during the swelling process of the zeolite precursor (Figure 4a−c). The resultant Pt@MCM-22 catalyst exhibits superior catalytic performance than those prepared by the impregnation and maintains 90% activity over five reaction-regeneration cycles.[65] To improve the encapsulation degree of Pt species in zeolite structure, the Pt species is introduced into the synthesis mixture of zeolite for hydrothermal crystallization.[66] As depicted in Figure 4d−f, The resultant K-PtSn@MFI catalyst contains subnanometer Pt clusters in the sinusoidal 10-ring channels of pure-silica MFI zeolite. The introduction of K and Sn can suppress the sintering during the high-temperature calcination procedure and modify the electronic properties of Pt clusters, respectively, resulting in the formation of highly stable and selective sites for PDH. Modifying the atomic structures of the PtSn clusters by postsynthesis treatments can cause one-order-magnitude variation in the deactivation rate for PDH, highlighting the sensitivity of the catalytic performance of PtSn clusters to their structural features, which are also proven by some recent studies based on theoretical modeling and kinetic measurements. For instance, variations in prereduction times lead to different degrees of interaction between Pt clusters and partially reduced Sn species, significantly influencing catalyst performance.[67] By precisely designing and synthesizing subnanometer Pt_xSn_y sites of different chemical compositions within the 10MR sinusoidal channels of pure-silica MFI zeolites, it is found that Pt_3Sn_1 sites exhibit the best C−H bond activation capability and the highest PDH activity among various structures. Additionally, the Pt_6Sn_x (x = 1, 2) sites demonstrated exceptional resistance to sintering and carbon deposition.[68] Due to its high reproducibility, the one-pot synthesis approach has been extended to many different combinations of Pt and cocatalyst metals, yielding a series of zeolite-encapsulated Pt catalysts for PDH with enhanced activity and stability than conventional Pt catalysts supported on open-structure surfaces.[69−74] In recent years, zeolite-encapsulated nonprecious metal catalysts prepared via one-pot method have also achieved excellent PDH catalytic performance. For example, through a ligand-stabilized one-pot method, Co species within a uniform MFI zeolite framework are constructed, forming the microstructure $(\equiv SiO)_2Co(HO-Si\equiv)_2$ sites.[54,75] This structure, through dynamic and continuous changes in electronic and coordination structures, effectively stabilized the C_3H_7 intermediate and facilitated the acceptance of H species, exhibiting exceptional PDH activity, selectivity, and stability compared to traditional impregnation and ion-exchange methods. Furthermore, the introduction of Na_2MoO_4 in the one-pot synthesis system has enabled precise control over the coordination structure of Co, establishing a new catalytic active center with an unsaturated tricoordinated cobalt unit ($(\equiv Si-O)CoO(O-Mo)$). The addition of Mo significantly enhances Co's ability to activate C−H bonds and promotes the desorption of propylene, exhibiting exceptionally high catalytic activity in the PDH reaction, not only surpassing all previously reported Co-based catalysts by nearly an order of magnitude but also exceeding the performance of most Pt-based catalysts under similar operational conditions.[53] We believe that by precisely controlling the active sites in subnanometer zeolite-encapsulated metal catalysts prepared via a one-pot method, the specific

https://doi.org/10.1021/jacsau.4c00730
JACS Au 2024, 4, 4084−4109

activity of the metal active sites and their long-term stability in alkane dehydrogenation reactions can be further improved. Regarding the practical application of this material in the industrial PDH process, one has to resolve the preparation of shaped zeolite-encapsulated Pt catalysts and mitigate the diffusion problems caused by the zeolite frameworks.

Although the physical confinement effect can enhance the stability and activity of catalysts, the diffusion limitations may increase the product's retention time, thereby triggering side reactions and catalyst deactivation. To address this issue, researchers can modify the morphology and pore structures of the supports. For instance, subnanometer Pt_4−O−Ge clusters supported on UTL-type zeolite, which possesses large pores composed of 14- and 12-ring channels (Figure 4g, h), demonstrate this approach. This unique property allows the catalyst to exhibit long-term stability under different space velocities for over 4500 h.[76]

Despite the faster diffusion originating from the larger pore structures or smaller dimensions in a specific direction, the catalyst's stability may be compromised by a reduction in crystal size and an increase in defective sites. This phenomenon is particularly detrimental in the presence of steam, where a large number of defects within the supports can lead to the migration and aggregation of active species. Therefore, choosing supports with complete crystallinity to enhance the stability of both support and active sites is also an effective strategy to improve activity.

2.5. Advanced Characterizations for PDH Catalysts

Characterization techniques bring new insights into the structure−activity relationship and help iteratively improve the PDH catalytic system by unraveling the deactivation mechanism. Established electron microscopy tools enable the visualization of support morphology and metal nanoparticles, and spectroscopy methods (including IR, UV−vis, Raman, and XAS) allow for the observation of variations in metal sites, intermediates, and carbon deposits.[77,78] However, advanced characterizations are required to discern the accurate structure of active sites and to explore the deactivation mechanism with high temporal and spatial resolutions.

In-situ and operando characterizations can seamlessly track the active site variation and coke formation. As shown in Figure 5a, in situ XANES reveals the chemical information during the dehydrogenation-regeneration cycles of the Pt−Sn/Al_2O_3 catalyst. During the temperature ramp to 600 °C under an H_2 flow, Pt−Sn/Al_2O_3 experiences the formation of metallic Pt and subsequent insertion of Sn to form Pt−Sn alloy. Oxygen treatment for coke burning clearly leads to the separation of Pt and Sn constituents, while the following H_2 reduction restores Pt−Sn alloy. Overall, the incorporation of Sn mitigates the Pt particle growth during the dehydrogenation-regeneration cycles, thus bringing prolonged stability and selectivity.[40] In another example, the CrO_x/Al_2O_3 catalyst is characterized by operando UV−vis and Raman spectroscopy integrated inside a pilot-scale reactor (Figure 5b). The operando UV−vis measures the color variations during the PDH cycles, correcting the Raman results for quantitative analysis. Based on the D_1/G ratio, the coke species increases with the temperature elevation, while the chemical composition is irrelevant to the position of the catalyst bed or reaction time.[79]

Advanced electron microscopy helps illustrate the definite structure of carefully designed catalysts. In the case of Pt−Sn clusters encapsulated in MFI zeolite, iDPC-STEM images demonstrate the accurate localization of subnanometric clusters in the sinusoidal channels. As shown in Figure 5c, Combining HAADF-STEM and iDPC images, along with DFT simulations, the structure of clusters was imaged, thus providing a new perspective for detecting the structure of PDH active sites and establishing structure−activity relationships.[66,68] However, with the state-of-the-art TEM technique, it is still very challenging to obtain images of the metal-zeolite interfaces with atomic resolution.

The coordination environment of the metal active sites can be deconvoluted from the X-ray pair distribution function (PDF), which collects both diffraction and scattering data and interprets atomic interactions in real space. For Ce/V NPs confined in mesopores SBA-15, PDF demonstrates a similar distribution curve with the simulated data, suggesting that the Ce/V structure remains intact when impregnated into the mesopores. The dispersion of Ce/V particles inside the SBA-15 channels enhances the TOF of oxidative PDH compared to bulk Ce/V cluster aggregates.[80] In another example, the PDF data of Fe/Al_2O_3 resembles the features of Fe_2O_3 within 5 Å, indicating the presence of highly dispersed Fe-phase on the alumina surface, instead of aluminate spinel ($FeAlO_3$) or larger Fe NPs.[81] Further, the satisfactory fitting results and the theoretical model prove the subnanometer Pt clusters within the germanium-containing MFI zeolite, changing its long-term symmetry due to the specific Pt positioning.[76] By correlating the PDF and EXAFS data acquired under reaction conditions, some insights on the activation and deactivation of the metal active sites could be obtained.

Furthermore, some advanced techniques are highly valuable but rarely applied in PDH investigations. For instance, inelastic neutron scattering technology indicates the formation of aromatic species in the used PDH catalyst, supplementing IR and Raman data in elucidating the composition of carbonaceous deposits.[82] Due to the strong interaction of neutrons with light elements, INS is suitable for investigating the hydrocarbon species on the catalysts, with various applications in propene oligomerization and methanol-to-olefin reactions.[83,84] In addition, X-ray computed tomography (CT) reveals the structure changes of the Pt−Ga bimetallic sites in the supported catalytically active liquid metal solutions (Figure 5d). X-ray CT provides a three-dimensional visualization of the catalyst structure before and after the PDH reaction, suggesting that the Pt-doped Ga particles evolve into Ga shells with Ga−Pt intermetallic constituents.[26] Other X-ray-based tomography methods include XRD-CT, XFR-CT, and STXM-CT, which may provide insightful information for the dynamic behaviors of the active sites and coke species. Besides, X-ray CT techniques are applicable for the energy- and spatial-resolved visualization of bulkier samples (micrometer to millimeter sizes), with high potential for investigating the catalysts in industrial scenarios.[85−87]

2.6. Outlook of Catalyst Design in PDH

By looking into the performance summary of recently reported materials for PDH, we can find that the noble metal catalysts are one- or two-order-magnitude higher than non-noble metal catalysts in PDH under similar conditions.[7,14] Noble metal catalysts may suffer fast catalyst deactivation due to coke deposition and the metal active sites usually suffer sintering issues after multiple reaction-regeneration cycles. In our opinion, the future directions of developing PDH catalysts based on noble metals mainly lie in the precise synthesis of

https://doi.org/10.1021/jacsau.4c00730
JACS Au 2024, 4, 4084−4109

subnanometer metal sites to maximize the utilization efficiency and activity of noble metal species. Another important direction is the catalyst's stability on the reaction stream and durability during multiple reaction-regeneration cycles. It is highly desirable to develop suitable solid carriers with appropriate porosity to limit the mobility of subnanometer noble metal sites in both oxidative and reduction atmospheres at high temperatures without compromising their accessibility to propane. In particular, it is important to achieve facile regeneration of the coked active sites by direct calcination in the presence of O_2 and to avoid the use of a Cl-containing atmosphere.

Regarding the non-noble metal catalysts, the major drawback is their intrinsically low capability for activating C−H bonds in light alkane molecules, leading to much lower space-time yields of propylene than the noble metal counterparts. One strategy to tackle this issue is to introduce very low amounts of noble metals as promotors for non-noble metal catalysts. For instance, incorporating hundreds of ppm of Pt into GaO_x/ZSM-5 catalyst leads to an improvement of specific activity for >20 times.[89] To further promote the synergy of atomically dispersed Pt species and the GaOx anchoring sites, it is necessary to optimize the synthesis methodology to precisely control the location of Pt species in the GaOx/ZSM-5 support. In general, the non-noble metal catalysts are more stable than the supported noble metal catalysts thanks to the strong bonding between metal active sites and the oxide carriers. The active sites may gradually sinter into metallic particles in a reductive atmosphere on the PDH reaction stream at high temperatures, resulting in catalyst deactivation and coke deposition. In some cases, the active sites can be generally restored after calcination treatment in air. However, the long-term stability of some recently reported systems (e.g., Ni@TiO_x, GaO_x/zeolite, ZnO/zeolite) still needs to be further verified.

3. GAP BETWEEN LABORATORY RESEARCH AND PRACTICAL PDH PROCESS

In contrast to fundamental research in the laboratory, industrial PDH processes typically employ pure propane as the reaction gas to maximize propane conversion efficiency. Previous studies indicate that the PDH using pure propane as the feed leads to extended catalyst lifetime at 500−550 °C, because the partial pressure of hydrogen also increases in the reaction mixture, slowing down the coke deposition and catalyst deactivation. Additionally, the hydrogen can react with the carbon deposits, further diminishing carbon accumulation on the catalyst surface.[61,90] However, industrial applications generally require higher temperatures (600−650 °C) to enhance propane conversion efficiency, and the elevated temperatures promote the coke deposition rates on the catalysts, necessitating periodic catalyst regeneration to restore the activity.[2,4,36,91] The industrial PDH process leverages moving bed technology for continuous catalyst regeneration, which offers the distinct advantage of uninterrupted operation and eliminates the need for process shutdowns.[2,4] Despite extensive research exploring a wide range of PDH catalyst carriers, such as zeolites, carbon materials, mesoporous silica, and CeO_2, their performance in practical applications often fails to match that of Al_2O_3 employed in established processes like Catofin and Oleflex. This discrepancy is primarily attributed to the higher mechanical strength and chemical stability of Al_2O_3 than other materials. In a moving bed reactor, the catalyst particles may break due to friction and collision if lacking mechanical strength, resulting in a decrease in reaction efficiency and potentially bed clogging and pressure drop. Furthermore, the relatively inert chemical nature of Al_2O_3 guarantees its structural robustness during long-term operation, preventing structural collapse during air calcination or in the presence of steam, thereby ensuring consistent performance and durability in industrial processes.[92−97]

Though the morphology, crystal structure, and acidity of Al_2O_3 support have been extensively explored, the Al_2O_3 catalysts developed in the academic community typically do not perform as well as those used in the Catofin and Oleflex processes. The disparity may originate from the complex structural characteristics of alumina itself, with nine different types of crystal structure, each exhibiting distinct atomic arrangements, acidity, porosity, surface area, and surface hydroxyl density (Figure 6).[98−100] While academia generally

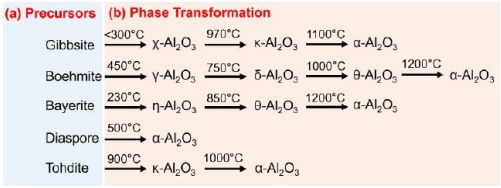

Figure 6. Phase transformation of $Al_2O_3$with different structures during the thermal treatments. Depending on the precursor and the treatment temperature, alumina with distinct crystallographic structures can be prepared.

prefers γ-Al_2O_3 as the carrier for PDH catalysts, other forms of alumina might possess advantages over γ-Al_2O_3 in some evaluation criteria. For example, γ-Al_2O_3 can be converted to θ-Al_2O_3 by calcination at higher temperatures, which exhibits higher thermal stability and lower hydroxyl content (lower acidity). This transformation results in less carbon accumulation and higher cyclic stability of Pt/θ-Al_2O_3 than the Pt/γ-Al_2O_3 counterpart. Nonetheless, θ-Al_2O_3 has relatively lower surface area and acidity, which adversely leads to lower dispersion of Pt and reduced catalytic activity.[101−104]

Besides crystallographic structures, Al_2O_3 displays various morphologies, including spheres, nanosheets, nanoflowers, and nanofibers, which offer numerous opportunities for tuning the metal-Al_2O_3 interfacial structures. Al_2O_3 materials with diverse morphologies can be prepared by various methods such as hydrothermal, sol−gel, precipitation, template, emulsion, microemulsion, and electrolysis.[105−107] Different morphologies impact the catalytic performance by enhancing mass transfer efficiency and stabilizing Pt nanoparticles through more five-coordinated Al^{3+} ions, which modify the electron structure of Pt and subsequently the activation process of propane C−H bonds.[108,109]

Adjusting synthesis parameters like aging time and temperature may also contribute to the performance of Al_2O_3-supported catalysts. For instance, by optimizing temperature gradients and elution conditions, Al_2O_3 microspheres with high mechanical strength are successfully synthesized through the low-carbon alcohol elution sol−gel method. The adsorption of low and high-carbon alcohols benefits the formation of a cross-linked network of fibers, thereby enhancing the mechanical strength of Al_2O_3.[110] Despite these innovations, the intricate synthesis process for Al_2O_3 often hinders academic research from achieving industrially relevant performance benchmarks. Considering the Al_2O_3 supports are used in shaped forms in the commercial processes and the metal active sites are introduced by impregnation, it is encouraged to perform shaping treatment

https://doi.org/10.1021/jacsau.4c00730
JACS Au 2024, 4, 4084−4109

of the as-prepared Al_2O_3 powder for the subsequent catalytic tests under conditions close to the commercial process.

In addition, the repeated redox regeneration processes always result in Al_2O_3 structure changes, which could significantly influence catalytic performance.[111] The exothermic heat from carbon combustion may cause changes in the acidic sites, hydroxyl groups, exposed crystal faces, Al coordination states, and even the crystal form of Al_2O_3.[112−114] Therefore, the thermal stability of Al_2O_3 is often a key factor, with numerous studies in recent years documenting the changes and improvements in thermal stability. However, in industrial applications, catalysts are not only subjected to high temperatures. For instance, during the reduction process, carbon burning, and even from moisture in the raw materials, alumina's structure is significantly affected. Under these conditions, Al_2O_3 is particularly prone to hydroxylation.[115−117] Such changes usually affect the metal's stability, a phenomenon observed in various active metals like Pt, Ag, and Cu, showing metal specificity.[41,118−121] To enhance the hydrothermal stability of Al_2O_3, the academic community employs strategies involving doping with metals and their oxides, as well as adjusting the conditions of hydrothermal synthesis or calcination, thereby modifying alumina's structure, surface hydroxyl group concentration, and crystallinity.[122−125] However, at present, few studies directly associate the hydrothermal stability of Al_2O_3 with the enhancement of PDH performance. Therefore, focusing on the hydrothermal stability of Al_2O_3 carriers and active sites will also be an important research direction in the future.

4. REGENERATION OF DEACTIVATED CATALYSTS

As mentioned before, the regeneration of deactivated catalysts is critical for the industrial PDH process due to the inevitable coke deposition. Regular regeneration of catalysts by burning off coke remains an indispensable procedure to ensure the continuous reaction in the moving bed reactor in the industrial process. However, frequent coke removal and regeneration processes may cause sintering or structure changes in the metal active sites and support, necessitating measures to redisperse the active sites. In this section, we will discuss the deactivated reasons and typical methods for the regeneration of the deactivated catalysts in PDH, and then compare the applicable scope of different methods as well as the associated technical issues.

4.1. Overview of the Deactivation Behaviors for the PDH Catalysts

The deactivation of PDH catalysts is typically caused by two main factors: first, changes or damage to the support structure; second, the aggregation of active metal sites.[126] The main reasons for changes or damage to the support structure include local overheating during repeated carbon removal and the detrimental effects of water formed during calcination or reduction processes. This impact may manifest as the above-mentioned structural changes or excessive hydroxylation of the open-space support like Al_2O_3, or as the collapse of the support in porous materials like zeolites under hydrothermal conditions, which reduces the surface area and leads to active metal sites sintering or coverage.[127]

Despite numerous studies aimed at enhancing the hydrothermal stability of many supports in recent years, there has been little direct focus on evaluating the hydrothermal stability of PDH catalysts.[128] However, methods intended to improve the hydrothermal stability of supports, when applied directly to the preparation of PDH catalysts, may have unknown effects on catalyst activity. Take zeolite as an example, common methods to enhance hydrothermal stability, such as crystallizing in a fluoride system or treating zeolites with silylating agents, can reduce structural defects and the number of internal and external silanol groups, thereby enhancing hydrothermal stability.[129−133] However, the excessive elimination of defects might also lead to the loss of sites stabling active metal and exacerbate metal sintering. Compared to these methods, doping with alkali metals and heteroatoms both inside or outside the framework may be more promising for preparing PDH catalysts with high hydrothermal stability.[134−139] It must be acknowledged, however, that once the properties of the support are altered or damaged, particularly in the presence of metal sites, such damage is difficult to reverse and is considered irreversible. Therefore, future research in this area, aimed at balancing hydrothermal stability and PDH activity to find the optimal solution, holds significant potential.

Another mode of deactivation, metal site sintering, is generally considered reversible and will be the focus of our subsequent discussion. Generally, aggregation and dispersion can be seen as a dynamic equilibrium process, which usually comprises two key processes: the disengagement of the metal species from the solid carrier and the capture of the mobile species at the anchoring sites. Normally, to achieve dispersion, the binding strength at the carrier sites for migrating metal species must be stronger than their tendency to aggregate. When the binding strength between metal species exceeds their interaction with the carrier, metal aggregation occurs.[126] The extent of this binding strength is closely related to the type of metal species, carriers, and treatment conditions (temperature, atmosphere, and time). In PDH catalysts, the sintering of active sites after multiple reaction-regeneration cycles is a common phenomenon for both noble and non-noble metal catalysts. Typically, due to cost considerations, industrial applications using non-noble metal catalysts (such as CrO_x or GaO_x-based catalysts) address sintering-induced deactivation by increasing reaction temperatures or replacing the catalyst.[1,4] However, given the high cost of noble metals, redispersion of the active sites has primarily been practised with noble metal catalysts, which will be the main topic of our subsequent discussion.

4.2. Oxidation/Reduction Redispersion Method

The oxidation/reduction method is the most convenient way for catalyst regeneration caused by coke deposition as demonstrated with a variety of supported metal catalysts made of Pd, Rh, Re, Ag, and Au.[126,140−152] In the case of supported Pt catalysts for PDH, treating a Pt/γ-Al_2O_3 catalyst at 500 °C in the air for 18 h triggers the oxidative redispersion of Pt, reducing the diameter of Pt particles from 10.7 to 4.1 nm.[152] The redispersion of Pt particles in an oxidative atmosphere at high temperatures is probably attributed to the formation of volatile PtO_x species, causing Pt atoms to detach from larger particles and migrate to the support.

However, under some circumstances, frequent oxidation/reduction regeneration processes can be one of the primary reasons for metal sintering instead of redispersion. This paradox is attributed to the perplexing effect of different atmospheres, processing times, and temperatures of sintering and redispersion. For example, a high Pt dispersion (70%) is achieved on Al_2O_3 support after oxidation at 550 °C, but severe sintering of Pt is observed when the temperature exceeds 600 °C due to the Ostwald ripening mechanism.[153] In the deactivated Pt catalysts containing coke deposits, the combustion of coke will cause local

https://doi.org/10.1021/jacsau.4c00730
JACS Au 2024, 4, 4084−4109

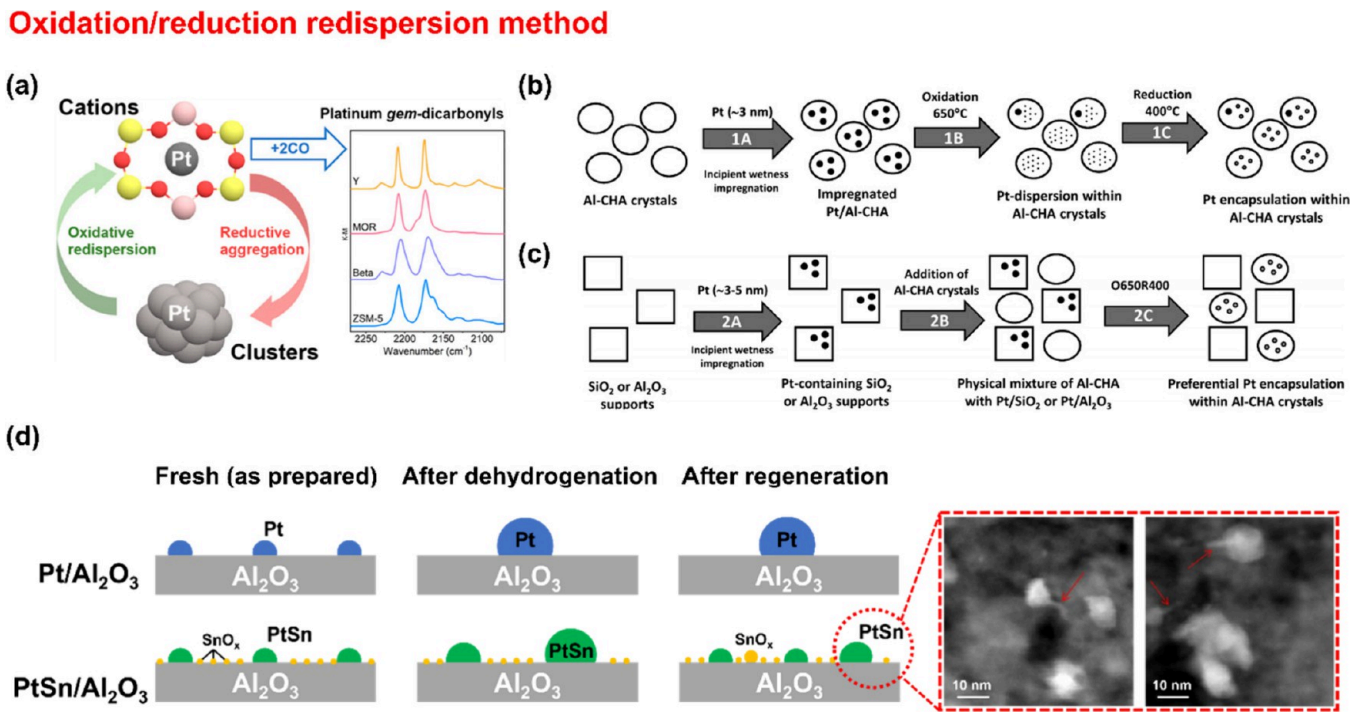

Figure 7. Regeneration of deactivation Pt catalysts by oxidation−reduction treatments. (a) Schematic illustration of the dispersion process of Pt species on aluminosilicate zeolites (Y, MOR, Beta, ZSM-5) during oxidation−reduction cyclic treatment. Taking ZSM-5 as an example, IR results show that Pt^{2+} ions are stabilized within the 6MR units of ZSM-5 zeolite with paired Al sites after calcination in air at 700 °C and the Pt^{2+} ions can be converted into Pt clusters after H_2 reduction treatment. Reproduced with permission from ref 155. Copyright 2016 American Chemical Society. (b) Schematic illustration of the atomic migration process of Pt nanoparticles on the outer surface of CHA zeolite. PtO_x species on the outer surface migrate into the CHA zeolite under after calcination treatment at 650 °C. (c) Schematic illustration of the migration process in the mechanical mixture of Pt/SiO_2 or Pt/Al_2O_3 with CHA zeolite. Pt species nearly migrate from the weakly interacting SiO_2 and Al_2O_3 to the CHA zeolite, as confirmed by TEM and EDS analysis. Reproduced with permission from ref 156. Copyright 2018 American Chemical Society. (d) Schematic illustration of the redispersion process of sintered Pt/Al_2O_3 and $PtSn/Al_2O_3$. As confirmed by TEM, Sn species act as the anchoring sites for Pt species. Reproduced with permission from ref 157. Copyright 2022 American Chemical Society.

hot spots within the catalyst particles, resulting in severe sintering of Pt species. In this sense, it is critical to select appropriate conditions for the oxidation−reduction treatments (temperature, time, partial pressure of O_2, and ramp rate in the heating procedure) to avoid or alleviate metal sintering.[89] In some cases, a high calcination temperature is mandatory for the removal of hard coke, resulting in the inevitable sintering of Pt species in the regeneration process.

As the metal particles grow larger, the redispersion of metal species becomes challenging because of the high stability of fully coordinated metal−metal bonding in the large metal particles.[154] Additionally, effective dispersion generally requires the presence of effective anchoring sites on the support, such as the Al sites on Al_2O_3 or aluminosilicate zeolites, alkali metal sites on pure silica supports, and metal promotors (Figure 7).[67,155−157] Otherwise, the high-temperature oxidation−reduction treatments may result in severe sintering due to Ostwald ripening as observed with Pt supported on alkali metal-free SiO_2.[158] Due to the lower volatility of RhO_x species than PtO_x, the sintering of Rh active sites during oxidation−reduction treatments should be easier to mitigate. Considering the remarkable performance reported with zeolite-encapsulated Rh catalysts, it is of interest to study the stability of Rh species during consecutive reaction-regeneration cycles.[39]

4.3. Oxychlorination Redispersion Method

Since metal chlorides exhibit higher mobility than oxides, the oxychlorination redispersion method can realize the redispersion of sintered catalysts when the conventional oxidation−reduction method is ineffective. Implied by the preparation of Pt/Al_2O_3 catalysts from chlorinated Pt sources (H_2PtCl_6 solution), the final Pt catalyst displays a better Pt dispersion compared to those prepared from other Pt precursors (such as $Pt(acac)_2$ and $Pt(NH_3)_4(NO_3)_2$). This superior dispersion is attributed to the decomposition of chloroplatinic acid during high-temperature calcination, producing HCl vapor that promotes the dispersion of Pt species on alumina,[159] which is validated by temperature-programmed reduction and UV−visible spectroscopy characterizations.[160,161]

The Cl-promoted metal dispersion can be further extended to restore the active sites in deactivated Pt catalysts. For instance, treating the Pt catalyst with mixture of gaseous chlorine compounds (e.g., Cl_2, HCl, dichloroethane, carbon tetrachloride, and other chlorinated hydrocarbons) and air can transform the metallic Pt particles into $Pt−O_x−Cl_y$ complexes.[162] According to the mechanistic study based on EXAFS measurements, O−Cl species are formed on the support surface during the oxychlorination treatment, while the Pt particles are transformed into $Pt−O_x−Cl_y$ complexes, which gradually migrate and become stabilized by the O−Cl sites on the support (Figure 8a).[163] While $Pt−O_x−Cl_y$ complexes are undoubtedly the key to achieving metal redispersion, descriptions of the specific structures of the intermediates vary across different studies and are influenced by multiple parameters. Variables such as temperature, chlorinating agent, oxygen/chlorine content, residence time, and reaction time significantly impact

https://doi.org/10.1021/jacsau.4c00730
JACS Au 2024, 4, 4084−4109

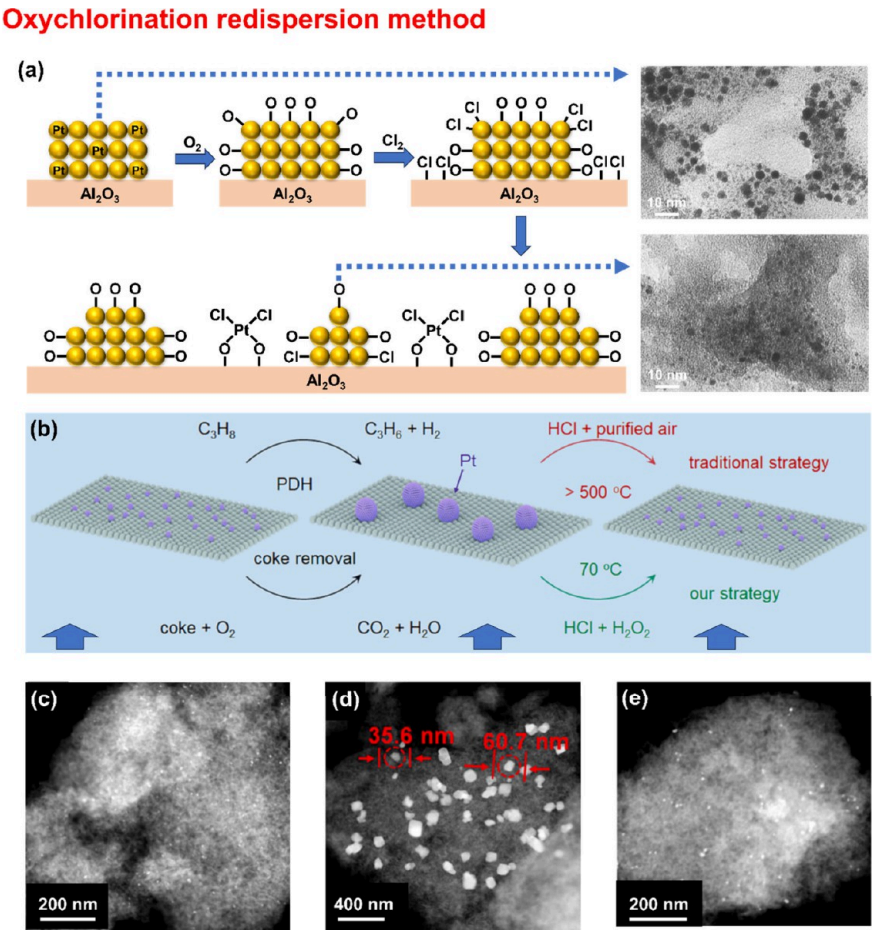

Figure 8. Regeneration of deactivation Pt catalysts by oxychlorination method. (a) Schematic illustration of the oxychlorination redispersion mechanism. The absorption peak around 340 nm in the UV−vis absorption spectrum corresponds to Pt−O_x−Cl_y species, with TEM confirming the redispersion process of the Pt species after oxychlorination treatment. Reproduced with permission from ref 163. Copyright 1996 American Chemical Society. (b) Schematic illustration of the regeneration process of sintered Pt at low temperatures with the help of H_2O_2 as strong oxidant. (c) HAADF-STEM image of fresh, (d) sintered, and (e) regenerated Pt−Ga_2O_3 through oxychlorination treatment. Reproduced with permission from ref 168. Copyright 2024 Elsevier.

the dispersion effect and its mechanism, among which temperature and chlorinating agents pose the most substantial influence on redispersion efficacy.

Typically, the redispersion phenomenon occurs within 500−600 °C, representing the optimal temperature range for the formation and migration of Pt−O_x−Cl_y complexes on the catalyst support.[160] With higher temperatures, despite the slightly enhanced dissociation of the chlorinated Pt compounds, the interactions between Pt−O_x−Cl_y complexes and the support are weakened, reducing redispersion efficacy and potentially leading to the formation of large Pt particles due to the self-decomposition of Pt−O_x−Cl_y complexes. Certainly, the conditions for oxychlorination treatment may vary with the physicochemical properties of the support. For instance, when Pt is loaded onto SiO_2 rather than Al_2O_3, lower temperatures are required to stabilize Pt−O_x−Cl_y complexes due to their weak interactions with SiO_2.[164,165]

Different chlorine dispersants, including Cl_2, HCl, CCl_4, and $C_2H_4Cl_2$, may participate in reactions via different mechanisms, resulting in distinct redispersion effects. Cl_2, one of the most employed chlorine sources in the industry, has been commercially applied for catalyst regeneration in the CCR regeneration unit of UOP's Oleflex process. Cl_2 dissociates into $Cl^\bullet$ radicals and reacts with PtO_2 to form Pt−O_x−Cl_y complexes through the following chemical transformations.

$$\text{Site} + Cl_2 \rightarrow \text{Cl–Site} \rightarrow \text{Site} + 2Cl^\bullet$$

$$(PtO_2)_x + 2Cl^\bullet \rightarrow (PtO_2)_{x-1}Pt(O{-}Cl)_2 \rightarrow (PtO_2)_{x-1} + Pt(O{-}Cl)_2$$

$$Pt{-}O{-}Cl \rightarrow [-O_{support}-] \rightarrow Pt{-}O{-}Cl{-}O_{support}$$

Due to the toxicity and storage challenges of Cl_2, researchers are exploring alternative chlorine dispersants.[166] For instance, HCl is a common alternative for Cl_2 in experimental research, but its high corrosiveness often necessitates the corrosion-resistant Hastelloy reactors and thereby significantly increases production costs.[167]

In addition to HCl, CCl_4, and $C_2H_4Cl_2$ are also applicable dispersants for oxychlorination reactions. Since the CCl_4 treatment primarily relies on its thermal decomposition reactions at higher temperatures (500−750 °C), incomplete decomposition of CCl_4 may occur at the typical oxychlorination temperature (around 500 °C). Introducing H_2O can improve CCl_4 utilization through the hydrolysis reaction, but it also produces corrosive $COCl_2$, which negatively affects the support

https://doi.org/10.1021/jacsau.4c00730
JACS Au 2024, 4, 4084−4109

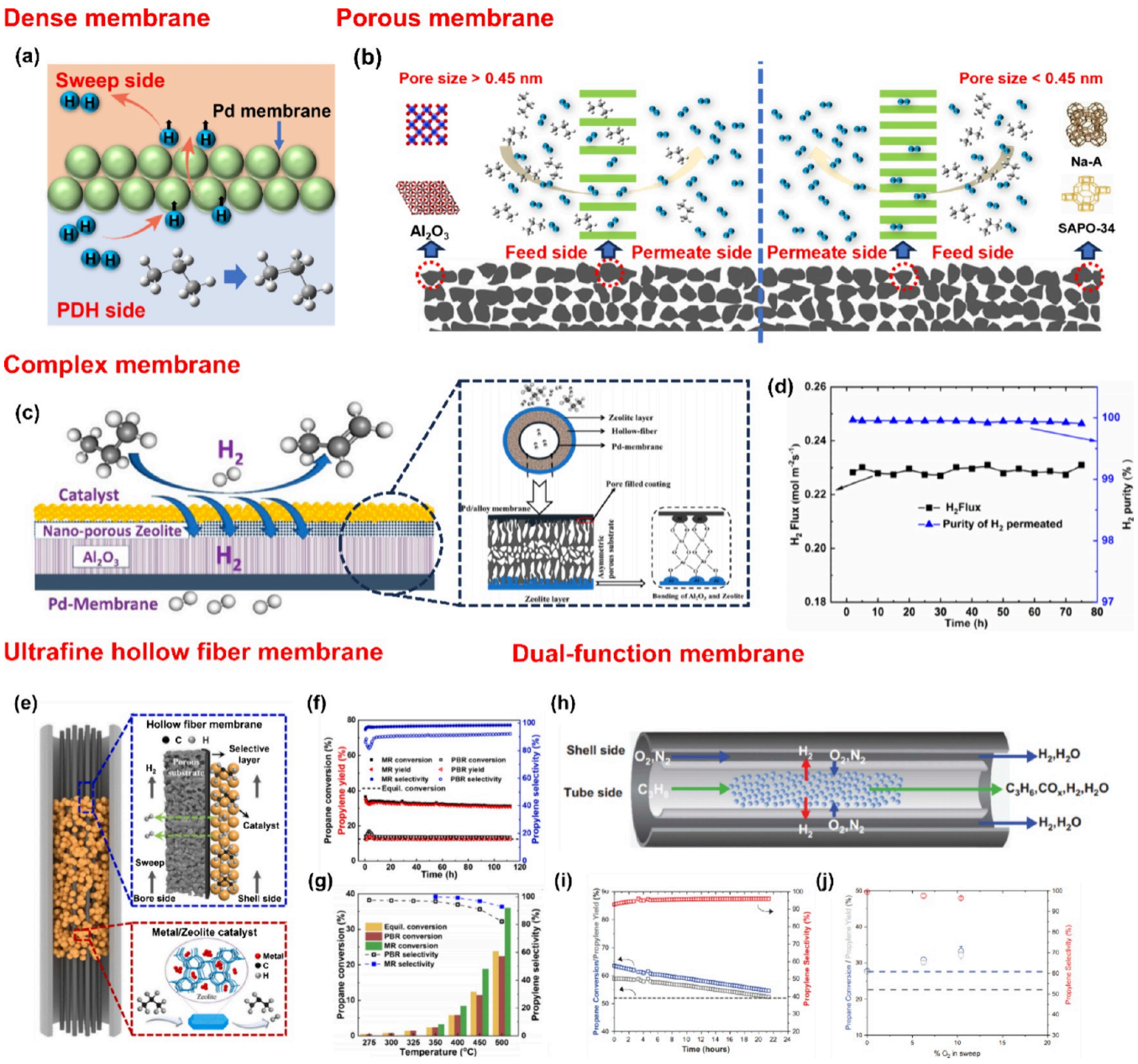

Figure 9. Design of membrane reactors for PDH. Schematic illustration of H_2 permeation mechanisms in (a) dense and (b) porous membranes. In porous membranes, hydrogen permeation occurs through a combination of diffusion and molecular sieving, allowing gas molecules to traverse the pores based on their size and kinetic interactions. SAPO-34 and Na-A zeolites, with typically uniform pore sizes <0.45 nm, exhibit excellent selectivity in H_2 separation from the reaction mixture of PDH. (c) Schematic illustration of the NaA−Pd-Al_2O_3 ternary composite membrane structure. (d) Stability test of the ternary composite membrane for H_2 separation. Reaction conditions: 10% C_3H_8 and C_3H_6 in H_2. Reproduced with permission from ref 207. Copyright 2020 American Chemical Society. (e) Schematic illustration of the CMS-MR H_2 selective separation process. (f) Long-term catalytic PDH performance in CMS-MR and PBR. (g) Catalytic PDH performance in CMS-MR and PBR at different temperatures. Reproduced with permission from ref 204. Copyright 2023 Cell Press. (h) Schematic illustration of a coupled catalyst-membrane system for PDH and H_2 oxidation. (i) PDH performance in MR. Dashed line: equilibrium limit. Reaction conditions: T = 580 °C, WHSV = 1.3 h^{-1}, sweep/feed flow = 10. (j) Relationship between C_3H_8 conversion and O_2 concentration. Black dashed line: equilibrium limit. Reaction conditions: T = 500 °C, WHSV = 0.86 h^{-1}, sweep/feed flow = 12. Reproduced with permission from ref 215. Copyright 2024 American Association for the Advancement of Science.

and metal active sites. Regarding the use of $C_2H_4Cl_2$ as the dispersant, $C_2H_4Cl_2$ tends to form coke on the catalyst surface through condensation reactions under oxygen-lean conditions.[164] Despite the fact that CCl_4 and $C_2H_4Cl_2$ are relatively safer than Cl_2, the practical application in industrial processes remains a challenge regarding minimizing equipment corrosion and harmful gas emissions.

In addition to changing the chlorine source, replacing the air with O_3 or H_2O_2 may also promote the redispersion process because of their stronger capability for oxidizing metallic Pt particles. For instance, utilizing H_2O_2 and HCl as dispersants to regenerate Pt-based catalysts at a mild temperature (70 °C), the regenerated catalyst demonstrates improved Pt dispersion, C_3H_8 conversion, and C_3H_6 selectivity (Figure 8b−e). So far, this method has been effectively implemented on benchmark PDH

https://doi.org/10.1021/jacsau.4c00730
JACS Au 2024, 4, 4084−4109

catalysts such as Pt−Sn/Al_2O_3 and Pt/Ga_2O_3 and has been validated on other metals including Pd, Au, Ir, Ru, and Rh.[168]

Although oxychlorination methods have been successfully applied in industrial processes for decades, their utilization still faces numerous issues. The usage of chlorinated compounds poses a significant threat to the environment, and the inevitable generation of HCl often causes equipment corrosion. While Hastelloy alloys can mitigate this corrosion, their high cost and long-term stability under harsh reaction conditions are series concerns. It is highly desired to develop new catalyst regeneration methods for redispersing large Pt particles without the involvement of HCl. More importantly, oxychlorination may not work effectively on support lacking sufficient anchoring sites for stabilizing the Pt−O_x−Cl_y intermediates. For instance, triggering oxychlorination redispersion effects on silica-supported Pt catalysts is particularly challenging and may result in exacerbated agglomeration.[159,169] Therefore, the industrial application of most currently developed Pt-based catalysts on pure silica supports (including SiO_2 and pure siliceous zeolite) is constrained by the redispersion of the sintered catalysts.

5. H_2 PERMEABLE MEMBRANE REACTORS FOR PDH

Due to thermodynamic constraints, PDH typically requires temperatures higher than 550 °C,[1,4,9] which often induces side reactions, such as cracking and coke formation.[170−172] As shown in the equation below, by selectively removing hydrogen to reduce the partial pressure of hydrogen (P_{H_2}), the forward PDH rate (R_C) can be greatly promoted, facilitating the efficient conversion of C_3H_8 at lower temperatures.[1,8,173] Therefore, compared to traditional fixed-bed reactors, membrane reactors, which enable the instant removal of H_2 from the reaction mixture, are capable of shifting the thermodynamic equilibrium of PDH, favoring the production of propylene under mild conditions.

$$R_C = k \times \left(P_{C_2H_6} - \frac{P_{C_2H_4} \times P_{H_2}}{K_{eq}} \right)$$

The efficiency of PDH in the membrane reactor is influenced by its operating parameters, such as sweep gas flow rate and pressure.[174] An increase in the sweep gas flow rate typically enhances the hydrogen recovery rate, boosting the forward PDH reaction rate. However, the growth in reaction rate is restricted by the accelerated carbon deposition on the catalyst and reaction membrane due to the depletion of H_2 in the reaction mixture.[175,176] Furthermore, an excessively high sweep gas flow can cause back-permeation to the feed side and decrease the partial pressure of C_3H_8, lowering conversion rates, and potentially lowering the selectivity to propylene.[177] Additionally, while raising the reaction pressure generally increases both H_2 permeation and overall reaction efficacy, it also risks hydrocarbon permeation through the membrane, potentially affecting the overall process efficiency.[178−180] In this section, we will discuss the applications of dense and porous membranes for constructing membrane reactors for PDH.

5.1. Dense H_2 Permeable Membranes

Dense membranes used in PDH include Pd-based alloy membranes and perovskite-based membranes.[181−183] Perovskite-based membranes are particularly noted for achieving efficient, high-purity hydrogen separation at temperatures exceeding 600 °C because the H_2 separation proceeds through an oxygen vacancies-assisted proton transport mechanism.[184] However, when adopting the perovskite-based membranes in PDH reactors, the working temperatures are usually set to around 500 °C for energy-saving considerations, resulting in declined H_2 separation efficiency. Unlike perovskite-based membranes, Pd-based alloy membranes, renowned for their high H_2 permeability and selectivity, function effectively at lower temperatures (below 500 °C).[185] In this case, H_2 adsorbs onto the surface of the Pd-based alloy membrane and dissociates into atomic hydrogen followed by diffusion through the membrane driven by a concentration gradient (Figure 9a). Upon reaching the opposite side, the atomic hydrogen recombines and subsequently desorbs from the surface, completing the hydrogen separation process.

While pure Pd membranes are highly effective in hydrogen separation, they are very expensive and vulnerable to several issues, including hydrogen embrittlement, deactivation, and poisoning. Hydrogen embrittlement arises when hydrogen atoms infiltrate into the Pd lattice, leading to internal stress and diminished membrane stability. Since palladium also possesses high reactivity in catalytic dehydrogenation reactions, deactivation is primarily induced by coke formation. Additionally, poisoning occurs due to impurities like CO, CO_2, and H_2S in the C_3H_8 feed, which strongly adsorb onto the Pd surface and markedly decrease its hydrogen permeability.[186] To mitigate these problems, researchers opt to improve the performance of pure Pd membranes by alloying them with other metals, including Ag, Cu, Au, Y, Zr, Nb, and V, thus developing more robust and efficient Pd-based alloy membranes.[174]

The PdAg alloy membrane is one of the most widely studied Pd-based membranes for hydrogen separation. Incorporating 23 wt % Ag into Pd membranes significantly enhances permeability and resistance to hydrogen embrittlement due to its stable face-centered cubic (FCC) structure, which undergoes minimal lattice changes upon hydrogen permeation and effectively minimizes stress.[187] Despite these improvements, PdAg alloys remain highly susceptible to sulfur poisoning, as the interaction with H_2S can form inactive compounds such as Pd_4S and $Ag_5Pd_{10}S_5$ on the alloy surface, substantially reducing permeability.[186,188] Additionally, PdAg membranes exhibit low chlorine tolerance, which is problematic during the chlorination regeneration process of Pt-based catalysts.[189] Besides doping with Ag, alloying Pd with Cu to form PdCu membranes provides commendable resistance to hydrogen embrittlement and sulfur poisoning while reducing the manufacturing cost, though the permeability is compromised.[185,190,191] Because of the weak dissociative adsorption of H_2S on Au, the sulfide formation on the surface of PdAu alloy membrane is suppressed, resulting in a marked diminishment of the adverse effects of H_2S-containing gases on hydrogen permeability.[192] Different from Cu, introducing gold increases the hydrogen permeation rate, but the high cost of gold restricts its broader application.[193−195]

Given that various bimetallic alloys invariably face certain issues, developing ternary or quaternary alloys may offer an advanced solution by combining the merits of individual elements. These membranes exhibit superior resistance to hydrogen embrittlement, poisoning, and carbon formation. For instance, PdAgAu membranes demonstrate up to three times the effective hydrogen permeability in comparison with PdAg and PdCu membranes in the presence of 20 ppm of H_2S.[196] However, issues like hydrogen embrittlement, poisoning, and deactivation remain unresolved in Pd-based alloy membranes, despite being partially mitigated. Further, catalyst regeneration processes like oxychlorination can damage Pd-based membranes

https://doi.org/10.1021/jacsau.4c00730
JACS Au 2024, 4, 4084−4109

and cause the segregation of the bimetallic or multimetallic membranes.

5.2. Porous H_2 Permeable Membranes

Porous membranes, the second most extensively researched type for PDH reactions, typically demonstrate enhanced stability in the presence of hydrocarbons in comparison with dense membranes. These porous materials include microporous SiO_2, porous Al_2O_3, zeolites, and various carbon-based materials.[197] Microporous silica membranes possess excellent hydrogen separation efficiency and stability at high temperatures, while their selectivity in separation is generally lower than other porous membranes (Figure 9b).[177] Additionally, the amorphous or partially crystalline structure of silica membranes are more prone to brittleness due to the breakage of Si−O bonds under moisture.[174] Despite the absence of water vapor formation in under ideal PDH conditions, the practical operation of PDH processes will introduce water vapor into the reactors because of catalyst activation with hydrogen gas, steam regeneration, or trace moisture in the propane feedstock. Hence, additions of transition metal oxides (like ZrO_x, NbO_x, NiO_x, TiO_x) or covalent organic linking agents are commonly employed to enhance the stability of SiO_2 membranes.[198−200] Additionally, while slightly more expensive, porous Al_2O_3 membranes can circumvent the thermal and steam instability issues of microporous SiO_2, challenges in precisely controlling pore size distribution hinder their ability to pose the efficient separation of H_2 from the reaction mixture.[177,201]

Zeolites, known for their crystalline structures with uniform pore architectures, offer higher H_2 selectivity than amorphous silica membranes (Figure 9b). Nevertheless, due to the close match between the kinetic diameters of C_3H_8 and C_3H_6 (0.45 nm) and the typical pore size range of zeolites, smaller pore sizes (≤0.45 nm) are essential for effective hydrogen separation in PDH. For example, Na-A type zeolite with a pore size of 0.41 nm and SAPO-34 zeolite with a pore size of 0.38 nm demonstrate high selectivity when separating C_3H_8, C_3H_6, and H_2.[202,203] Despite these advantages, the selectivity remains lower than that of dense membranes, especially at high temperatures. Furthermore, while zeolite and microporous silica membranes mitigate carbon deposition deactivation commonly observed in Pd-based metal membranes, they are susceptible to another deactivation mechanism where byproducts from PDH such as benzene, toluene, cyclohexane, and xylene undergo capillary condensation and coadsorption on the membrane surface, obstructing the pore structure and diminishing H_2 permeability.[174] Besides, due to the presence of acid sites in the zeolites, the coke deposition rate in zeolite membranes can be higher than that on amorphous silica membranes.

Carbonaceous materials, particularly carbon molecular sieve membranes, are highly suitable for PDH due to their exceptional mechanical strength, high thermal stability, and superior selectivity.[204] However, their production complexity and high cost pose significant challenges for large-scale industrial deployment.[61] In addition, carbon material membranes are specifically vulnerable during catalyst regeneration procedures involving calcination in air for removal of carbon deposits. Although some catalysts can be regenerated under a reductive atmosphere like H_2, the efficiency in carbon removal is much lower than that by calcination in air.[205] Consequently, addressing the regeneration challenges of catalysts in membrane reactors based on carbon materials remains a critical challenge.

Since dense and porous membranes have demonstrated individual merits and defects in promoting PDH reactions, combining these two membrane structures into a composite may leverage their unique advantages and further enhance the separation efficiency. For instance, Pd-based alloy membranes typically require a minimum thickness of 20 μm to deliver sufficient mechanical strength. However, hydrogen permeability inversely correlates with membrane thickness, meaning excessive thickness reduces hydrogen flux and increases Pd usage, substantially increasing production costs.[206] By integrating Pd-based alloy membranes with porous materials like Vycor glass, ceramic molecular sieves, porous SiO_2, and metallic substrates, the thickness of the Pd-based alloy layer can be reduced to less than 1 μm, significantly increasing its permeability and decreasing the manufacturing cost. Moreover, forming a composite Pd membrane is an effective strategy to inhibit carbon deposition. For example, by depositing Na-A zeolite and Pd membranes on the opposite sides of an Al_2O_3 hollow fiber support, the resultant sandwich-structured membrane exhibits excellent anticoking properties and hydrogen separation efficiency at 600 °C (Figure 9c, d).[207−209] Nonetheless, composite membranes encounter notable challenges, including poor adhesion and the migration of metal elements between these layers, potentially leading to decreased permeability and membrane deformation.[210−212]

5.3. Design of the Membrane Reactor Structure

In addition to tuning the membrane's composition, modifying the microstructures of the membrane reactors represents a pivotal approach toward high device performance. Membrane reactors constructed by coating catalyst powder onto the membrane surfaces based on hollow fibers demonstrate superior performance than conventional packed-bed membrane reactors. They also exhibit enhanced mass transfer and catalyst utilization efficiency due to a vast membrane surface area and close integration with the catalyst. For instance, through the combination of a PtZn/S-1 catalyst with an ultrafine carbon molecular sieve (CMS) hollow carbon fiber membrane reactor (315 μm outer diameter), the catalytic system achieves tripled conversion efficiency than the conventional packed bed reactor while maintaining high selectivity to propylene (Figure 9e−g). Moreover, the excellent thermal conductivity enables the hollow carbon fiber membrane reactor to uniform Joule heating, opening the possibility of using renewable electricity as an input energy source. Currently, the intricate and costly fabrication process of ultrafine hollow carbon fiber membrane reactors and their long-term stability presents challenges to their commercial adoption.[204]

In recent years, dual-function membrane reactors, which enhance conversion efficiency by facilitating distinct reactions on each membrane side, have emerged as a promising direction in the field of membrane reactor engineering. Specifically, in membrane systems for PDH, the sweep gas on one side reacts with H_2 permeate from the dehydrogenation side, lowering hydrogen concentration and boosting its separation.[213,214] For example, employing the separated hydrogen for CO_2 methanation reaction can not only consume H_2 for shifting the equilibrium but also promote the utilization of H_2. Meanwhile, the CO_2 sweeping process is devoid of the risks of reverse permeation. Even if it were to occur, the permeated CO_2 can be effectively utilized within the CO_2-assisted PDH process, reducing coke formation and promoting catalyst stability.[3,6,10,11] Similarly, in the absence of coupled reactions, a SiO_2/Al_2O_3

https://doi.org/10.1021/jacsau.4c00730
JACS Au 2024, 4, 4084−4109

complex hollow fiber membrane with Pt_1Sn_1/SiO_2 catalyst incorporated son the PDH side, achieves a C_3H_8 conversion rate exceeding 40% of the equilibrium conversion (Figure 9h–j). Further, coupling the endothermic PDH reaction (tube side) with the exothermic H_2 oxidation reaction (shell side), the H_2 permeation and C_3H_8 conversion rate are effectively enhanced, while the heating energy required for the reaction is significantly reduced. By introducing 10% O_2, the system displays a conversion rate exceeding 55% of the equilibrium conversion. The permeated O_2 can also be utilized in the O_2-assisted PDH process, effectively reducing coke formation. Although dual-function membrane reactors hold great promise, their commercialization requires extensive research on catalysts and reactor designs to ensure optimal performances.[215]

When designing the alkane dehydrogenation system based on a membrane reactor, one needs to carefully consider the interfacial structure between the catalyst layer and the gas-diffusion membrane. Close contact between the catalyst layer can favor the efficiently extracting gas from the reaction mixture but may affect the gas permeability. Furthermore, the coke deposited on the catalyst layer may also cause the blocking of the gas-diffusion membrane. If so, the membrane reactor may need to be subjected to a regeneration treatment, which may cause the structural deformation of the catalyst layer and membrane interface.

6. NEW CONCEPTS IN PROCESS DESIGN FOR PDH

Although significant progress has been achieved in the reactor and catalyst design for PDH, the substantial energy consumption, unfavorable thermodynamic constraints, and the resultant CO_2 emissions have not been significantly alleviated. Furthermore, the catalysts inevitably suffer deactivation issues caused by coking and metal sintering under high-temperature reaction conditions. Researchers have been exploring alternative strategies to achieve propane conversion under milder conditions through chemical looping, photoassisted, electric field-assisted, and microwave-assisted approaches.[216]

Chemical looping refers to the technology of using reducible metal oxides as solid oxygen carriers to selectively consume hydrogen through lattice oxygen. This technology selectively removes hydrogen from the product, driving the reaction equilibrium toward propylene formation and effectively addressing the issue of frequent regeneration of PDH catalysts caused by carbon deposition. Compared to direct oxidative dehydrogenation, this approach avoids the risks of propylene overoxidation to CO_2, the high energy consumption in product separation, and the explosion hazards associated with the addition of oxygen.[217,218] Currently, the feasibility of oxygen carriers such as Bi_2O_3, In_2O_3, V_2O_5, Fe_2O_3, MoO_3, and CeO_2-doped materials has been widely validated.[219−224] However, the poor redox stability, low oxygen storage capacity, and limited hydrogen combustion selectivity of these carriers remain obstacles to their commercial application. Moreover, the complexity of the system makes it difficult to precisely control the interaction between dehydrogenation sites and hydrogen combustion sites at the molecular level to achieve a synergistic match between propane dehydrogenation and selective hydrogen combustion reactions. To address these issues, a $FeVO_4$–VO_x chemical looping selective hydrogen combustion and PDH tandem reaction system has been proposed, demonstrating excellent cycle stability, oxygen storage capacity, and selectivity. This system consists of VO_x loaded on γ-Al_2O_3 as a catalyst and a synthetic $FeVO_4$ oxygen carrier. During the reaction, the VO_x catalyst promotes the dissociation of hydrogen and the $FeVO_4$ oxygen carrier provides lattice oxygen to convert hydrogen into water, significantly enhancing the efficiency of propane dehydrogenation. As the lattice oxygen in $FeVO_4$ is gradually consumed, the driving force for hydrogen combustion weakens. At this point, the reduced oxygen carrier is exposed to air in an oxidation reactor to replenish its lattice oxygen, completing the chemical looping process. Although this process improves efficiency, it must be acknowledged that the limited capacity of solid oxides to store lattice oxygen requires frequent regeneration, which could affect the sustainability and efficiency of the reaction.

Utilizing renewable solar light for PDH offers a distinct advantage over traditional thermal catalysis by surpassing thermodynamic constraints to enable the reaction under mild conditions, thereby substantially decreasing the energy consumption and operational costs, while concurrently mitigating catalyst deactivation issues commonly induced by elevated temperatures.[225,226] For example, employing ZnO as support embedded with PdZn intermetallic particles can achieve a 54.0 mmol g_{cata}^{-1} h^{-1} C_3H_6 production rate and 89.4% selectivity to propylene. The PDH activity, superior to previously reported photocatalysts, is ascribed to the lattice oxygen sites generated by light illumination on ZnO, which can efficiently activate the inert C–H bonds of C_3H_8. Compared to Pd nanoparticles, PdZn promotes the removal and replenishment cycle of lattice oxygen due to its strong electronic interaction with the ZnO support.[216] However, due to the inherent stability of the sp^3 C–H bonds and their lower electron affinity, the currently reported PDH photocatalysts show low efficiencies, especially under visible light irradiation. A recently reported Pt/black TiO_2 catalyst exhibits high PDH performance under visible to near-infrared light irradiation. Experimental results and theoretical calculations indicate that the strong interaction between black TiO_2 and Pt facilitates effective interfacial charge transfer.[227] However, despite this breakthrough in photocatalytic PDH driven by visible light, the C_3H_6 production rates of the photocatalytic systems remain unsatisfactory. Therefore, tuning the local atomic structure of specific photoactive sites for C–H bond activation and selecting supports with enhanced optical properties and interfacial charge transfer to utilize low-energy visible or even infrared light for efficient PDH will be a promising direction. Besides, from a reactor engineering point of view, it is a challenge to manage the heat transfer and temperature distribution in a photothermal reactor for PDH at high temperatures.

Photothermal catalysis technology is also considered a promising approach to surpass the thermodynamic limit of PDH. Unlike photocatalysis, photothermal catalysis requires some external heating to enhance the efficiency of the PDH process.[228−231] The provided heat facilitates the effective utilization of high-energy photons, thereby boosting their capacity to activate C–H bonds. For instance, V/TiO_2 catalyst successfully achieved 42 μmol·g^{-1}·h^{-1} C_3H_6 production rate under UV light irradiation at 500 °C, which is a 9.2% improvement over the test performed under traditional thermal heating conditions. This enhancement is claimed to be associated with the formation of more electron-deficient V atoms under UV light irradiation, significantly promoting the activation of C_3H_8.[232]

Additionally, a more advanced concept of photothermal catalysis recently has been proposed based on the nanogreenhouse effect and plasmonic hybridization effect to directly utilize

https://doi.org/10.1021/jacsau.4c00730
JACS Au 2024, 4, 4084–4109

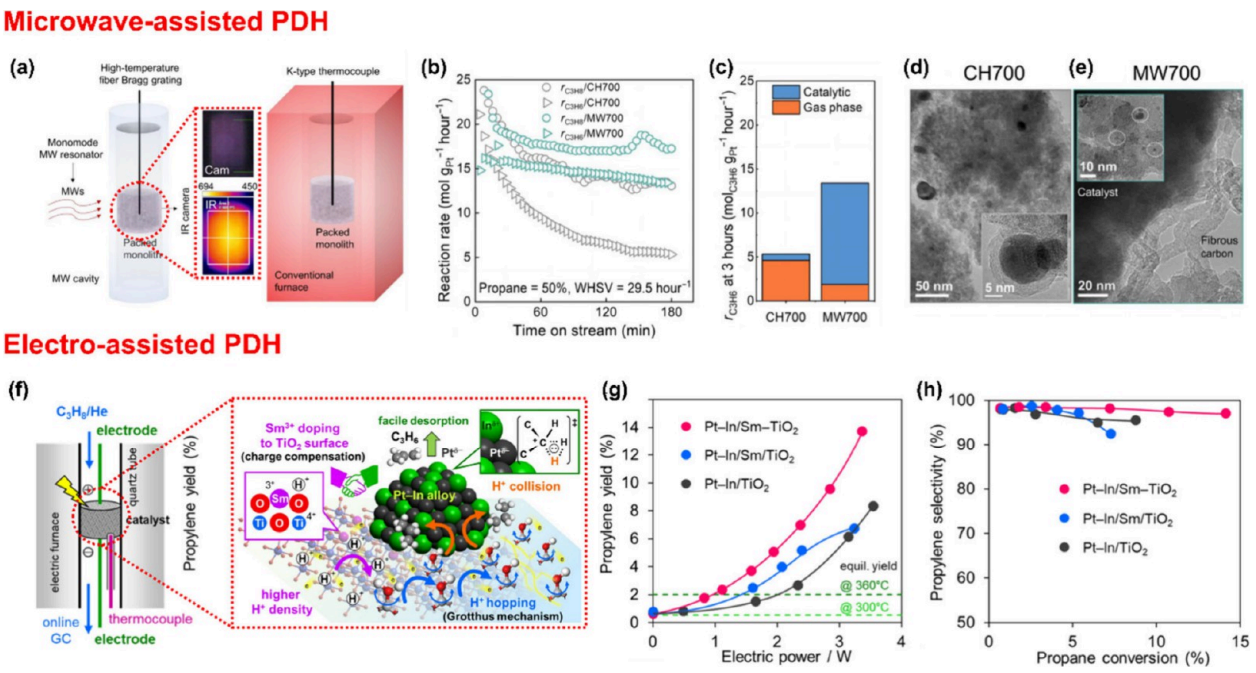

Figure 10. | New concepts in design of PDH processes. (a) Schematic illustration of the microwave-assisted (MW) and conventional heating (CH) PDH reactor. (b) Catalytic performances of a typical PtSn/SiO_2 catalyst in CH and MW reactors. (c) Contribution ratio of catalytic and gas-phase PDH in CH and MW reactors. The catalytic PDH reaction predominantly occurred in the MW reactor, while the gas-phase PDH reaction was in CH reactors. TEM images of the PtSn/SiO_2 catalyst after PDH tests in the (d) CH and (e) MW reactor at 700 °C. In the CH reactor, the Pt particles exhibit significant aggregation with carbon deposition, whereas, in the MW reactor, the Pt particles show high dispersion and carbon deposition mainly occurs on the support. Reproduced with permission from ref 239. Copyright 2023 American Association for the Advancement of Science. (f) Schematic illustration of the electric field-assisted PDH reactor and catalytic mechanism. The PDH catalytic performance of Sm-PtIn/TiO_2. (g) C_3H_8 conversion and (h) C_3H_6 selectivity. The reaction furnace temperature was fixed at 300 °C. The green dashed lines represent the thermodynamic equilibrium yields of C_3H_6 at temperatures of 300 and 360 °C. Reproduced with permission from ref 244. Copyright 2023 Wiley-VCH.

UV−vis light to heat the support and/or the active metal surface.[233] For instance, the plasmonic superstructure of ultrasmall Co nanoparticles on sandwich-structure Co-ss@SiO_2 catalysts are heated from room temperature to 300 °C within just 2 min of light exposure, demonstrating superior photothermal conversion performance compared to other catalysts.[234] This novel photothermal catalysis concept has been reported for use in the photothermal hydrogenation of CO_2.[235,236] This concept can be extended to the design of supported metal catalysts for PDH, in which the active sites for propane activation can be immobilized on a solid carrier that enables the conversion of light into heat. Photocatalytic processes typically require transition metal semiconductors like TiO_2 or ZnO, which can generate photoinduced electrons and holes under light irradiation. For photothermal catalysis, active sites producing plasmonic resonance, such as Co or Ni sites and PtCo or PtNi alloy, are crucial for activating C−H bonds and driving the reaction by generating high local temperatures through the energy from light.[233,237,238]

Microwave-assisted PDH addresses the limitations of traditional tube furnace heating, in which a temperature gradient may exist between the tube wall and the catalyst particles. Microwave triggers rapid and uniform heating of the catalyst bed, significantly reducing energy consumption. In the case of PtSn/SiO_2, employing a microwave-assisted method for PDH demonstrates higher reaction activity and selectivity than in fixed-bed reactors while substantially reducing coke formation rates (Figure 10a−e).[239] In traditional fixed-bed reactors, simultaneous heating of the catalyst and surrounding gases leads to hydrocarbon cracking and polymerization in the gas phase, forming coke even in the absence of contact with the Pt sites. In contrast, microwave heating selectively heats the catalyst, causing coke to deposit primarily near the Pt sites. Additionally, due to the insulating properties of SiO_2, heating primarily occurs at the Pt sites, rather than the SiO_2 support, therefore reducing the surface energy and possibility of the Pt agglomeration. However, the electromagnetic field generated by the microwaves tends to concentrate at the contact points between catalyst particles or the ends of the catalysts, resulting in local overheating and subsequent metal sintering.[240] In the future, utilizing metals such as Co/Ni, which have high microwave absorption efficiency, as active sites or alloying them with Pt may lead to composite catalysts for the microwave-assisted PDH process. The microwave heating directly heats the local active sites surrounded by the microwave absorbents, which may induce synergistic effects between metals and carriers different from traditional thermal catalysis. For example, this interaction could influence the migration of carbonaceous species on the carriers. Exploring the mechanisms and guiding the synthesis of catalysts with new ideas will be an intriguing area of research.

Electric field-assisted PDH is also a highly attractive catalytic system operating at relatively low temperatures (<300 °C). Applying an electric field to the catalyst enhances the migration of protons formed from the cleavage of C−H bonds on Pt particles and significantly lowers the barriers for C−H activation and H_2 recombination in the PDH reaction, therefore breaking the thermodynamic equilibrium limitations and enhancing propane conversion efficiency at low reaction temperatures. Moreover, the decrease in reaction temperature suppresses coke

https://doi.org/10.1021/jacsau.4c00730
JACS Au 2024, 4, 4084−4109

formation and extends the catalyst lifetime.[241,242] For instance, applying electric field-assisted PDH on Pt−In/TiO_2 demonstrates a C_3H_6 yield of 10.2% at 250 °C, which is 2 orders of magnitude higher than the 0.1% yield under traditional thermal reaction conditions (Figure 10f−h).[243] Alloying with In adjusts Pt's electronic and geometric structures, thus contributing to the stabilization of the cationic transition states and $C_3H_7^+$ intermediate, increasing the selectivity for C_3H_6. In addition, introducing Sm to the TiO_2 support increases the number of surface hydroxyl groups, which promotes C_3H_8 conversion efficiency and achieves a C_3H_6 yield of 19.3% at 300 °C, in comparison to ∼8% obtained with the Sm-free PtIn/TiO_2. Despite these promising results, electric field-assisted PDH methods typically exhibit lower selectivity than traditional thermal PDH due to the side reactions such as C−C cracking promoted by the electric fields.[244]

In addition to the strengths and drawbacks mentioned above, photoassisted, photothermal-assisted, microwave-assisted, and electric field-assisted methods are only practiced in small reactors and the scaling up of these techniques is more difficult than the conventional thermal reactors. For industrial-scale fixed-bed continuous reactors, especially photocatalytic systems, their application is limited by the difficulty of light penetration through traditional bed layers, necessitating the use of thin-layer catalysts. Aside from an in-depth understanding of the structure-performance relationship of solid catalysts in the presence of external fields for PDH, the large-scale application of the above new PDH technologies also requires substantial progress in reactor engineering for coupling the solid catalysts and external energy resources in a scalable manner. The microscale heat transfer and management in the composite catalysts and macroscale heat management in the reactor have not been systematically studied yet.

7. PERSPECTIVES

Despite the high number of publications on the development of new PDH catalysts, the industry has not adopted any novel catalysts in the commercial processes. This is attributable to the substantial differences between laboratory-scale studies and industrial processes in terms of the reaction conditions. In the industrial process, higher temperatures (>600 °C) and pure C_3H_8 are typically employed to achieve high C_3H_8 production rates while the catalysts in a large portion of fundamental studies are tested at 550−600 °C using diluted propane as the reaction feed. The discrepancies in the reaction conditions may affect the translation of the results obtained in fundamental studies into practical applications.[245,246]

Moreover, the large discrepancies in the testing conditions in different studies preclude the formation of a unified understanding of the structure-performance relationship. In principle, the activities of different catalysts can be directly compared based on the turnover frequencies (TOFs) measured under the same conditions. However, it is not practical to compare TOFs among different catalysts under industrially relevant conditions because of the diffusion limitations. The reaction rate for the propane dehydrogenation reaction is greatly dependent on the reaction conditions (e.g., partial pressure of the propane in the feed gas, reaction temperature, and w8 h space velocity) and propane conversion levels. Therefore, it would be unfair to compare the performances of Pt-based catalysts under different testing conditions by directly calculating the reaction rates according to the activity data reported in the literature. In recent years, the academic community has begun using a new parameter, "k_f", to compare the PDH activity of different catalysts. This parameter represents the contribution of the normalized active site to the PDH forward reaction rate. The calculation of "k_f" takes into account various factors including the partial pressure of propane, dilution with hydrogen or inert gases, catalysts bed height, volume expansion coefficient, and space velocity. Compared to the reaction rates derived from the conversion levels measured in the catalytic tests, k_f can be applied to comparing different catalysts tested at high conversion levels.[35,59] Besides specific activity, the deactivation rate is also a key criterion that is associated with the catalyst's stability under the reaction conditions. Most of the reported works calculate the deactivation rate/constant by assuming the catalyst follows a first-order decay pattern, which again will be greatly affected by the reaction conditions. For a given catalyst, the deactivation constant could vary in a range of one-order magnitude when changing the feed composition (i.e., the partial pressure of propane in the reaction feed). At the current stage, it is suggested to present the catalytic performances obtained under different reaction conditions by varying the reaction temperature and feed composition, which will be very helpful for achieving a balanced comparison with previous works and the data obtained under comparable conditions can also serve as high-quality training sets for data-driven catalyst discovery in future studies.

Additionally, industrial PDH reactions often utilize moving-bed reactors to achieve continuous reaction-regeneration operations for the removal of the coke in the deactivated metal catalysts, necessitating the use of shaped solid carriers with high mechanical strength. However, most of the carrier materials developed by academia typically fail to match the mechanical strength of commercial Al_2O_3 used in Catofin and Oleflex processes. Achieving high mechanical strength in Al_2O_3 supports necessitates in-depth research into the surface structures, morphology, porosity, defects and coordination environment of the surface Al sites in the Al_2O_3 support. Evaluating the performance of supported metal catalysts in powder form is an efficient way for screening the candidate materials while it is highly encouraged to perform catalytic evaluations on shaped catalysts instead of powder samples to further evaluate the catalyst's potential for practical application. When dealing with solid catalysts in shaped form, multiscale (from nanometer to micrometer scale) characterizations are suggested to clarify the influence of the spatial distribution of the active sites and their evolution under reaction conditions.[247]

Moreover, the frequent regeneration of catalysts to remove carbon deposits can lead to the aggregation of active metal sites. Oxidative regeneration and oxychlorination regeneration are mainstream methods for regenerating sintered catalysts. However, the conditions for metal particle redispersion vary significantly across different catalysts, and inappropriate treatment temperature and time can lead to more severe sintering. It is of great necessity to explore the redispersion method of sintered metal catalysts on zeolite-based supports to push the recently reported zeolite-supported metal catalysts toward industrial applications. The rational selection of appropriate regeneration protocol relies on the multiscale characterizations of the structural evolution of metal species on the solid carriers in both powder and shaped forms. In particular, it is necessary to develop suitable accelerated aging method to study the potential structural transformations of metal active sites under long-term reaction conditions.

https://doi.org/10.1021/jacsau.4c00730
JACS Au 2024, 4, 4084−4109

Considering the relatively high maturity of the PDH processes, the knowledge and experiences accumulated in the research of PDH can be in principle translated to other alkane dehydrogenation reactions, such as dehydrogenation of long-chain alkanes for the production of long-chain alkenes and dehydrogenation of cycloalkanes for H_2 storage applications.[248] In the context of the transition of the conventional systems based on fossil resources to the new energy systems based on renewable energy resources, the above-mentioned alkane dehydrogenation reactions may play critical roles in the sustainable production of chemicals and large-scale utilization of green H_2. On the one hand, the lessons on the design and controllable preparation of supported noble metal catalysts with high catalytic efficiencies can be directly translated into the design of advanced catalysts in other alkane dehydrogenation reactions for lowering the usage of noble metals. On the other hand, the optimized structural configuration of the active sites may vary with the target reactions because of the differences in the reactivities of the alkane substrates. For instance, in the case of dehydrogenation of long-chain alkanes, it is essential to choose appropriate support for the metal function components to minimize the production of aromatic byproducts. Regarding the dehydrogenation of cycloalkanes, it is crucial to suppress the undesired C−C cleavage reaction toward the production of gaseous byproducts so that the H_2 released from the dehydrogenation process can meet the purity requirements for fuel cell applications. Moreover, elucidating the structure−reactivity relationship in PDH catalysts is also very helpful for the rational design of bifunctional catalysts for dehydroaromatization of light alkanes and anaerobic ammodehydrogenation of ethane to acetonitrile.[249,250] Therefore, for the emerging alkane dehydrogenation reactions, the catalyst design principles should be established by combining the historical accumulation from PDH research studies and the technical features of the target processes.

AUTHOR INFORMATION

Corresponding Author

Lichen Liu − *Engineering Research Center of Advanced Rare Earth Materials, Department of Chemistry, Tsinghua University, Beijing 100084, China;* orcid.org/0000-0001-5067-0481; Email: lichenliu@mail.tsinghua.edu.cn

Authors

Zhe He − *Engineering Research Center of Advanced Rare Earth Materials, Department of Chemistry, Tsinghua University, Beijing 100084, China*

Jingnan Yang − *Engineering Research Center of Advanced Rare Earth Materials, Department of Chemistry, Tsinghua University, Beijing 100084, China*

Complete contact information is available at: https://pubs.acs.org/10.1021/jacsau.4c00730

Notes

The authors declare no competing financial interest.

ACKNOWLEDGMENTS

L.L. thanks the financial support from the National Natural Science Foundation of China (22272087), the National Key R&D Program of China (2022YFA1503901), and Tsinghua University from the Tsinghua-Jiangyin Innovation Special Fund (TJISF, 20222000555).

REFERENCES

(1) Sattler, J. J. H. B.; Ruiz-Martinez, J.; Santillan-Jimenez, E.; Weckhuysen, B. M. Catalytic Dehydrogenation of Light Alkanes on Metals and Metal Oxides. *Chem. Rev.* **2014**, *114* (20), 10613−10653.

(2) Chen, S.; Chang, X.; Sun, G.; Zhang, T.; Xu, Y.; Wang, Y.; Pei, C.; Gong, J. Propane dehydrogenation: catalyst development, new chemistry, and emerging technologies. *Chem. Soc. Rev.* **2021**, *50* (5), 3315−3354.

(3) Atanga, M. A.; Rezaei, F.; Jawad, A.; Fitch, M. W.; Rownaghi, A. A. Oxidative dehydrogenation of propane to propylene with carbon dioxide. *Applied Catalysis B: environmental* **2018**, *220*, 429−445.

(4) Carter, J. H.; Bere, T.; Pitchers, J. R.; Hewes, D. G.; Vandegehuchte, B. D.; Kiely, C. J.; Taylor, S. H.; Hutchings, G. J. Direct and oxidative dehydrogenation of propane: from catalyst design to industrial application. *Green Chem.* **2021**, *23* (24), 9747−9799.

(5) Hu, Z.-P.; Yang, D.; Wang, Z.; Yuan, Z.-Y. State-of-the-art catalysts for direct dehydrogenation of propane to propylene. *Chinese Journal of Catalysis* **2019**, *40* (9), 1233−1254.

(6) Bian, K.; Zhang, G.; Zhu, J.; Wang, X.; Wang, M.; Lou, F.; Liu, Y.; Song, C.; Guo, X. Promoting Propane Dehydrogenation with CO2 over the PtFe Bimetallic Catalyst by Eliminating the Non-selective Fe(0) Phase. *ACS Catal.* **2022**, *12* (11), 6559−6569.

(7) Sun, M.-L.; Hu, Z.-P.; Wang, H.-Y.; Suo, Y.-J.; Yuan, Z.-Y. Design Strategies of Stable Catalysts for Propane Dehydrogenation to Propylene. *ACS Catal.* **2023**, *13* (7), 4719−4741.

(8) Nawaz, Z. Light alkane dehydrogenation to light olefin technologies: a comprehensive review. *Reviews in Chemical Engineering* **2015**, *31* (5), 413−436.

(9) Docherty, S. R.; Rochlitz, L.; Payard, P.-A.; Copéret, C. Heterogeneous alkane dehydrogenation catalysts investigated via a surface organometallic chemistry approach. *Chem. Soc. Rev.* **2021**, *50* (9), 5806−5822.

(10) Jiang, X.; Sharma, L.; Fung, V.; Park, S. J.; Jones, C. W.; Sumpter, B. G.; Baltrusaitis, J.; Wu, Z. Oxidative Dehydrogenation of Propane to Propylene with Soft Oxidants via Heterogeneous Catalysis. *ACS Catal.* **2021**, *11* (4), 2182−2234.

(11) Carrero, C. A.; Schloegl, R.; Wachs, I. E.; Schomaecker, R. Critical Literature Review of the Kinetics for the Oxidative Dehydrogenation of Propane over Well-Defined Supported Vanadium Oxide Catalysts. *ACS Catal.* **2014**, *4* (10), 3357−3380.

(12) Tan, S.; Hu, B.; Kim, W.-G.; Pang, S. H.; Moore, J. S.; Liu, Y.; Dixit, R. S.; Pendergast, J. G.; Sholl, D. S.; Nair, S.; Jones, C. W. Propane Dehydrogenation over Alumina-Supported Iron/Phosphorus Catalysts: Structural Evolution of Iron Species Leading to High Activity and Propylene Selectivity. *ACS Catal.* **2016**, *6* (9), 5673−5683.

(13) Sarazen, M. L.; Jones, C. W. MOF-Derived Iron Catalysts for Nonoxidative Propane Dehydrogenation. *J. Phys. Chem. C* **2018**, *122* (50), 28637−28644.

(14) Song, S.; Sun, Y.; Yang, K.; Fo, Y.; Ji, X.; Su, H.; Li, Z.; Xu, C.; Huang, G.; Liu, J.; Song, W. Recent Progress in Metal-Molecular Sieve Catalysts for Propane Dehydrogenation. *ACS Catal.* **2023**, *13* (9), 6044−6067.

(15) Wang, Y.; Suo, Y.; Ren, J.-T.; Wang, Z.; Yuan, Z.-Y. Spatially isolated cobalt oxide sites derived from MOFs for direct propane dehydrogenation. *J. Colloid Interface Sci.* **2021**, *594*, 113−121.

(16) Zhao, D.; Tian, X.; Doronkin, D. E.; Han, S.; Kondratenko, V. A.; Grunwaldt, J.-D.; Perechodjuk, A.; Vuong, T. H.; Rabeah, J.; Eckelt, R.; Rodemerck, U.; Linke, D.; Jiang, G.; Jiao, H.; Kondratenko, E. V. In situ formation of ZnOx species for efficient propane dehydrogenation. *Nature* **2021**, *599* (7884), 234−238.

(17) Hu, P.; Lang, W.-Z.; Yan, X.; Chu, L.-F.; Guo, Y.-J. Influence of gelation and calcination temperature on the structure-performance of porous VOX-SiO2 solids in non-oxidative propane dehydrogenation. *J. Catal.* **2018**, *358*, 108−117.

(18) Chang, Q.-Y.; Wang, K.-Q.; Sui, Z.-J.; Zhou, X.-G.; Chen, D.; Yuan, W.-K.; Zhu, Y.-A. Rational Design of Single-Atom-Doped Ga2O3 Catalysts for Propane Dehydrogenation: Breaking through Volcano Plot by Lewis Acid-Base Interactions. *ACS Catal.* **2021**, *11* (9), 5135−5147.

(19) Liu, H.; Zhou, J.; Chen, T.; Hu, P.; Xiong, C.; Sun, Q.; Chen, S.; Lo, T. W. B.; Ji, H. Isolated Pt Species Anchored by Hierarchical-like Heteroatomic Fe-Silicalite-1 Catalyze Propane Dehydrogenation near the Thermodynamic Limit. *ACS Catal.* **2023**, *13* (5), 2928−2936.
(20) Wang, G.; Zhang, H.; Wang, H.; Zhu, Q.; Li, C.; Shan, H. The role of metallic Sn species in catalytic dehydrogenation of propane: Active component rather than only promoter. *J. Catal.* **2016**, *344*, 606−608.
(21) Raman, N.; Maisel, S.; Grabau, M.; Taccardi, N.; Debuschewitz, J.; Wolf, M.; Wittkämper, H.; Bauer, T.; Wu, M.; Haumann, M.; Papp, C.; Görling, A.; Spiecker, E.; Libuda, J.; Steinrück, H.-P.; Wasserscheid, P. Highly Effective Propane Dehydrogenation Using Ga-Rh Supported Catalytically Active Liquid Metal Solutions. *ACS Catal.* **2019**, *9* (10), 9499−9507.
(22) Phadke, N. M.; Mansoor, E.; Bondil, M.; Head-Gordon, M.; Bell, A. T. Mechanism and Kinetics of Propane Dehydrogenation and Cracking over Ga/H-MFI Prepared via Vapor-Phase Exchange of H-MFI with GaCl3. *J. Am. Chem. Soc.* **2019**, *141* (4), 1614−1627.
(23) Yang, T.; Zhong, Y.; Li, J.; Ma, R.; Yan, H.; Liu, Y.; He, Y.; Li, D. Construction of a Unique Structure of Ru Sites in the RuP Structure for Propane Dehydrogenation. *ACS Appl. Mater. Interfaces* **2021**, *13* (28), 33045−33055.
(24) Jiang, F.; Zeng, L.; Li, S.; Liu, G.; Wang, S.; Gong, J. Propane Dehydrogenation over Pt/TiO2-Al2O3 Catalysts. *ACS Catal.* **2015**, *5* (1), 438−447.
(25) Wang, T.; Jiang, F.; Liu, G.; Zeng, L.; Zhao, Z.-j.; Gong, J. Effects of Ga doping on Pt/CeO2-Al2O3 catalysts for propane dehydrogenation. *AIChE J.* **2016**, *62* (12), 4365−4376.
(26) Jaegers, N. R.; Danghyan, V.; Shangguan, J.; Lizandara-Pueyo, C.; Deshlahra, P.; Iglesia, E. Heterolytic C-H Activation Routes in Catalytic Dehydrogenation of Light Alkanes on Lewis Acid-Base Pairs at ZrO2 Surfaces. *J. Am. Chem. Soc.* **2024**, *146* (37), 25710−25726.
(27) Zhang, Y.; Zhao, Y.; Otroshchenko, T.; Lund, H.; Pohl, M.-M.; Rodemerck, U.; Linke, D.; Jiao, H.; Jiang, G.; Kondratenko, E. V. Control of coordinatively unsaturated Zr sites in ZrO2 for efficient C-H bond activation. *Nat. Commun.* **2018**, *9* (1), 3794.
(28) Wang, J.; Chang, X.; Chen, S.; Sun, G.; Zhou, X.; Vovk, E.; Yang, Y.; Deng, W.; Zhao, Z.-J.; Mu, R.; Pei, C.; Gong, J. On the Role of Sn Segregation of Pt-Sn Catalysts for Propane Dehydrogenation. *ACS Catal.* **2021**, *11* (8), 4401−4410.
(29) Singh, J.; Nelson, R. C.; Vicente, B. C.; Scott, S. L.; van Bokhoven, J. A. Electronic structure of alumina-supported monometallic Pt and bimetallic PtSn catalysts under hydrogen and carbon monoxide environment. *Phys. Chem. Chem. Phys.* **2010**, *12* (21), 5668−5677.
(30) Takigawa, I.; Shimizu, K.-i.; Tsuda, K.; Takakusagi, S. Machine-learning prediction of the d-band center for metals and bimetals. *RSC Adv.* **2016**, *6* (58), 52587−52595.
(31) Yang, M.-L.; Zhu, Y.-A.; Zhou, X.-G.; Sui, Z.-J.; Chen, D. First-Principles Calculations of Propane Dehydrogenation over PtSn Catalysts. *ACS Catal.* **2012**, *2* (6), 1247−1258.
(32) Cybulskis, V. J.; Bukowski, B. C.; Tseng, H.-T.; Gallagher, J. R.; Wu, Z.; Wegener, E.; Kropf, A. J.; Ravel, B.; Ribeiro, F. H.; Greeley, J.; Miller, J. T. Zinc Promotion of Platinum for Catalytic Light Alkane Dehydrogenation: Insights into Geometric and Electronic Effects. *ACS Catal.* **2017**, *7* (6), 4173−4181.
(33) Wang, P.; Liao, H.; Chen, Y.; Tao, X.; Gan, Y.; Deng, H.; Fu, Y.; Tang, Y.; Wu, L.; Tan, L. Enhanced PtIn Catalyst via Ce-Assisted Confinement Effect in Propane Dehydrogenation. *ACS Catal.* **2024**, *14* (11), 8116−8129.
(34) Wang, P.; Yang, M.; Liao, H.; Xu, K.; Zong, X.; Xie, Z.; Zhao, H.; Xu, Y.; Yang, H.; Gan, Y.; Fang, Y.; Wu, L.; Tang, Y.; Tan, L. Restructured zeolites anchoring singly dispersed bimetallic platinum and zinc catalysts for propane dehydrogenation. *Cell Reports Physical Science* **2023**, *4* (3), 101311.
(35) Motagamwala, A. H.; Almallahi, R.; Wortman, J.; Igenegbai, V. O.; Linic, S. Stable and selective catalysts for propane dehydrogenation operating at thermodynamic limit. *Science* **2021**, *373* (6551), 217−222.
(36) Wang, Y.; Hu, P.; Yang, J.; Zhu, Y.-A.; Chen, D. C-H bond activation in light alkanes: a theoretical perspective. *Chem. Soc. Rev.* **2021**, *50* (7), 4299−4358.
(37) Au, C.-T.; Ng, C.-F.; Liao, M.-S. Methane Dissociation and Syngas Formation on Ru, Os, Rh, Ir, Pd, Pt, Cu, Ag, and Au: A Theoretical Study. *J. Catal.* **1999**, *185* (1), 12−22.
(38) Hannagan, R. T.; Giannakakis, G.; Réocreux, R.; Schumann, J.; Finzel, J.; Wang, Y.; Michaelides, A.; Deshlahra, P.; Christopher, P.; Flytzani-Stephanopoulos, M.; Stamatakis, M.; Sykes, E. C. H. First-principles design of a single-atom-alloy propane dehydrogenation catalyst. *Science* **2021**, *372* (6549), 1444−1447.
(39) Zeng, L.; Cheng, K.; Sun, F.; Fan, Q.; Li, L.; Zhang, Q.; Wei, Y.; Zhou, W.; Kang, J.; Zhang, Q.; Chen, M.; Liu, Q.; Zhang, L.; Huang, J.; Cheng, J.; Jiang, Z.; Fu, G.; Wang, Y. Stable anchoring of single rhodium atoms by indium in zeolite alkane dehydrogenation catalysts. *Science* **2024**, *383* (6686), 998−1004.
(40) Iglesias-Juez, A.; Beale, A. M.; Maaijen, K.; Weng, T. C.; Glatzel, P.; Weckhuysen, B. M. A combined in situ time-resolved UV-Vis, Raman and high-energy resolution X-ray absorption spectroscopy study on the deactivation behavior of Pt and PtSn propane dehydrogenation catalysts under industrial reaction conditions. *J. Catal.* **2010**, *276* (2), 268−279.
(41) Zhou, S.-Z.; Li, W.-C.; He, B.; Xie, Y.-D.; Wang, H.; Liu, X.; Chen, L.; Wei, J.; Lu, A.-H. An Active and Regenerable Nanometric High-Entropy Catalyst for Efficient Propane Dehydrogenation. *Angew. Chem., Int. Ed.* **2024**, No. e202410835.
(42) Nakaya, Y.; Hayashida, E.; Asakura, H.; Takakusagi, S.; Yasumura, S.; Shimizu, K.-i.; Furukawa, S. High-Entropy Intermetallics Serve Ultrastable Single-Atom Pt for Propane Dehydrogenation. *J. Am. Chem. Soc.* **2022**, *144* (35), 15944−15953.
(43) Xing, F.; Ma, J.; Shimizu, K.-i.; Furukawa, S. High-entropy intermetallics on ceria as efficient catalysts for the oxidative dehydrogenation of propane using CO2. *Nat. Commun.* **2022**, *13* (1), 5065.
(44) Chang, X.; Zhao, Z.-J.; Lu, Z.; Chen, S.; Luo, R.; Zha, S.; Li, L.; Sun, G.; Pei, C.; Gong, J. Designing single-site alloy catalysts using a degree-of-isolation descriptor. *Nat. Nanotechnol.* **2023**, *18* (6), 611−616.
(45) Sun, G.; Zhao, Z.-J.; Mu, R.; Zha, S.; Li, L.; Chen, S.; Zang, K.; Luo, J.; Li, Z.; Purdy, S. C.; Kropf, A. J.; Miller, J. T.; Zeng, L.; Gong, J. Breaking the scaling relationship via thermally stable Pt/Cu single atom alloys for catalytic dehydrogenation. *Nat. Commun.* **2018**, *9* (1), 4454.
(46) Liu, X.; Wang, X.; Zhen, S.; Sun, G.; Pei, C.; Zhao, Z.-J.; Gong, J. Support stabilized PtCu single-atom alloys for propane dehydrogenation. *Chemical Science* **2022**, *13* (33), 9537−9543.
(47) Dai, Y.; Gao, X.; Wang, Q.; Wan, X.; Zhou, C.; Yang, Y. Recent progress in heterogeneous metal and metal oxide catalysts for direct dehydrogenation of ethane and propane. *Chem. Soc. Rev.* **2021**, *50* (9), 5590−5630.
(48) Liu, G.; Zeng, L.; Zhao, Z.-J.; Tian, H.; Wu, T.; Gong, J. Platinum-Modified ZnO/Al2O3 for Propane Dehydrogenation: Minimized Platinum Usage and Improved Catalytic Stability. *ACS Catal.* **2016**, *6* (4), 2158−2162.
(49) Yuan, Y.; Zhao, Z.; Lobo, R. F.; Xu, B. Site Diversity and Mechanism of Metal-Exchanged Zeolite Catalyzed Non-Oxidative Propane Dehydrogenation. *Advanced Science* **2023**, *10* (13), 2207756.
(50) Phadke, N. M.; Mansoor, E.; Head-Gordon, M.; Bell, A. T. Mechanism and Kinetics of Light Alkane Dehydrogenation and Cracking over Isolated Ga Species in Ga/H-MFI. *ACS Catal.* **2021**, *11* (4), 2062−2075.
(51) Yuan, Y.; Lobo, R. F.; Xu, B. Ga2O22+ Stabilized by Paired Framework Al Atoms in MFI: A Highly Reactive Site in Nonoxidative Propane Dehydrogenation. *ACS Catal.* **2022**, *12* (3), 1775−1783.
(52) Huang, M.; Maeno, Z.; Toyao, T.; Shimizu, K.-i. Ga speciation and ethane dehydrogenation catalysis of Ga-CHA and MOR: Comparative investigation with Ga-MFI. *Catal. Today* **2023**, *411*−*412*, 113824.
(53) Qu, Z.; He, G.; Zhang, T.; Fan, Y.; Guo, Y.; Hu, M.; Xu, J.; Ma, Y.; Zhang, J.; Fan, W.; Sun, Q.; Mei, D.; Yu, J. Tricoordinated Single-Atom

https://doi.org/10.1021/jacsau.4c00730
JACS Au 2024, 4, 4084−4109

Cobalt in Zeolite Boosting Propane Dehydrogenation. *J. Am. Chem. Soc.* **2024**, *146* (13), 8939−8948.
(54) Hu, Z.-P.; Qin, G.; Han, J.; Zhang, W.; Wang, N.; Zheng, Y.; Jiang, Q.; Ji, T.; Yuan, Z.-Y.; Xiao, J.; Wei, Y.; Liu, Z. Atomic Insight into the Local Structure and Microenvironment of Isolated Co-Motifs in MFI Zeolite Frameworks for Propane Dehydrogenation. *J. Am. Chem. Soc.* **2022**, *144* (27), 12127−12137.
(55) Zhang, T.; Pei, C.; Sun, G.; Chen, S.; Zhao, Z.-J.; Sun, S.; Lu, Z.; Xu, Y.; Gong, J. Synergistic Mechanism of Platinum-GaOx Catalysts for Propane Dehydrogenation. *Angew. Chem., Int. Ed.* **2022**, *61* (35), No. e202201453.
(56) Sattler, J. J. H. B.; Gonzalez-Jimenez, I. D.; Luo, L.; Stears, B. A.; Malek, A.; Barton, D. G.; Kilos, B. A.; Kaminsky, M. P.; Verhoeven, T. W. G. M.; Koers, E. J.; Baldus, M.; Weckhuysen, B. M. Platinum-Promoted Ga/Al2O3 as Highly Active, Selective, and Stable Catalyst for the Dehydrogenation of Propane. *Angew. Chem., Int. Ed.* **2014**, *53* (35), 9251−9256.
(57) van Deelen, T. W.; Hernández Mejía, C.; de Jong, K. P. Control of metal-support interactions in heterogeneous catalysts to enhance activity and selectivity. *Nature Catalysis* **2019**, *2* (11), 955−970.
(58) Hu, Z.-P.; Wang, Z.; Yuan, Z.-Y. Cr/Al2O3 catalysts with strong metal-support interactions for stable catalytic dehydrogenation of propane to propylene. *Molecular Catalysis* **2020**, *493*, 111052.
(59) Qi, L.; Babucci, M.; Zhang, Y.; Lund, A.; Liu, L.; Li, J.; Chen, Y.; Hoffman, A. S.; Bare, S. R.; Han, Y.; Gates, B. C.; Bell, A. T. Propane Dehydrogenation Catalyzed by Isolated Pt Atoms in ≡SiOZn-OH Nests in Dealuminated Zeolite Beta. *J. Am. Chem. Soc.* **2021**, *143* (50), 21364−21378.
(60) Qi, L.; Zhang, Y.; Babucci, M.; Chen, C.; Lu, P.; Li, J.; Dun, C.; Hoffman, A. S.; Urban, J. J.; Tsapatsis, M.; Bare, S. R.; Han, Y.; Gates, B. C.; Bell, A. T. Dehydrogenation of Propane and n-Butane Catalyzed by Isolated PtZn4 Sites Supported on Self-Pillared Zeolite Pentasil Nanosheets. *ACS Catal.* **2022**, *12* (18), 11177−11189.
(61) Chai, Y.; Chen, S.; Chen, Y.; Wei, F.; Cao, L.; Lin, J.; Li, L.; Liu, X.; Lin, S.; Wang, X.; Zhang, T. Dual-Atom Catalyst with N-Colligated Zn1Co1 Species as Dominant Active Sites for Propane Dehydrogenation. *J. Am. Chem. Soc.* **2024**, *146* (1), 263−273.
(62) Szeto, K. C.; Jones, Z. R.; Merle, N.; Rios, C.; Gallo, A.; Le Quemener, F.; Delevoye, L.; Gauvin, R. M.; Scott, S. L.; Taoufik, M. A Strong Support Effect in Selective Propane Dehydrogenation Catalyzed by Ga(i-Bu)3 Grafted onto γ-Alumina and Silica. *ACS Catal.* **2018**, *8* (8), 7566−7577.
(63) Xu, Z.; Xu, R.; Yue, Y.; Yuan, P.; Bao, X.; Abou-Hamad, E.; Basset, J.-M.; Zhu, H. Bimetallic Pt-Sn nanocluster from the hydrogenolysis of a well-defined surface compound consisting of [(AlO)Pt(COD)Me] and [(AlO)SnPh3] fragments for propane dehydrogenation. *J. Catal.* **2019**, *374*, 391−400.
(64) Chen, S.; Xu, Y.; Chang, X.; Pan, Y.; Sun, G.; Wang, X.; Fu, D.; Pei, C.; Zhao, Z.-J.; Su, D.; Gong, J. Defective TiOx overlayers catalyze propane dehydrogenation promoted by base metals. *Science* **2024**, *385* (6706), 295−300.
(65) Liu, L.; Díaz, U.; Arenal, R.; Agostini, G.; Concepción, P.; Corma, A. Generation of subnanometric platinum with high stability during transformation of a 2D zeolite into 3D. *Nat. Mater.* **2017**, *16* (1), 132−138.
(66) Liu, L.; Lopez-Haro, M.; Lopes, C. W.; Li, C.; Concepcion, P.; Simonelli, L.; Calvino, J. J.; Corma, A. Regioselective generation and reactivity control of subnanometric platinum clusters in zeolites for high-temperature catalysis. *Nat. Mater.* **2019**, *18* (8), 866−873.
(67) Liu, L.; Lopez-Haro, M.; Lopes, C. W.; Rojas-Buzo, S.; Concepcion, P.; Manzorro, R.; Simonelli, L.; Sattler, A.; Serna, P.; Calvino, J. J.; Corma, A. Structural modulation and direct measurement of subnanometric bimetallic PtSn clusters confined in zeolites. *Nature Catalysis* **2020**, *3* (8), 628−638.
(68) Dou, X.; Li, W.; Zhang, K.; Hou, H.; He, Z.; Zhu, C.; Meira, D. M.; Lopez-Haro, M.; Xia, Z.; He, P.; Xiao, H.; Liu, L. Size-Dependent Structural Features of Subnanometer PtSn Catalysts Encapsulated in Zeolite for Alkane Dehydrogenation. *ACS Catal.* **2024**, *14* (5), 2859−2871.
(69) Wang, Y.; Hu, Z.-P.; Lv, X.; Chen, L.; Yuan, Z.-Y. Ultrasmall PtZn bimetallic nanoclusters encapsulated in silicalite-1 zeolite with superior performance for propane dehydrogenation. *J. Catal.* **2020**, *385*, 61−69.
(70) Zhou, J.; Liu, H.; Xiong, C.; Hu, P.; Wang, H.; Wang, X.; Ji, H. Potassium-promoted Pt-In bimetallic clusters encapsulated in silicalite-1 zeolite for efficient propane dehydrogenation. *Chemical Engineering Journal* **2023**, *455*, 139794.
(71) Qu, Z.; Zhang, T.; Yin, X.; Zhang, J.; Xiong, X.; Sun, Q. Zeolite-encaged Ultrasmall Pt-Zn Species with Trace Amount of Pt for Efficient Propane Dehydrogenation. *Chemical Research in Chinese Universities* **2023**, *39* (6), 870−876.
(72) Luo, L.; Zhou, T.; Li, W.; Li, X.; Yan, H.; Chen, W.; Xu, Q.; Hu, S.; Ma, C.; Bao, J.; Pao, C.-W.; Wang, Z.; Li, H.; Ma, X.; Luo, L.; Zeng, J. Close Intimacy between PtIn Clusters and Zeolite Channels for Ultrastability toward Propane Dehydrogenation. *Nano Lett.* **2024**, *24* (24), 7236−7243.
(73) Zhang, B.; Li, G.; Zhai, Z.; Chen, D.; Tian, Y.; Yang, R.; Wang, L.; Zhang, X.; Liu, G. PtZn intermetallic nanoalloy encapsulated in silicalite-1 for propane dehydrogenation. *AIChE J.* **2021**, *67* (7), No. e17295.
(74) Sun, Q.; Wang, N.; Fan, Q.; Zeng, L.; Mayoral, A.; Miao, S.; Yang, R.; Jiang, Z.; Zhou, W.; Zhang, J.; et al. Subnanometer bimetallic platinum-zinc clusters in zeolites for propane dehydrogenation. *Angew. Chem.* **2020**, *132* (44), 19618−19627.
(75) Wu, X.; Song, S.; Yang, M.; Zhang, P.; Xu, C.; Wei, Y.; Huang, G.; Liu, J.; Song, W. The Microenvironment Change of Isolated Co Sites in Silicalite-1 Zeolite Induced by Balancing Cations for Boosting Propane Dehydrogenation. *Chem. Mater.* **2023**, *35* (18), 7789−7799.
(76) Ma, Y.; Song, S.; Liu, C.; Liu, L.; Zhang, L.; Zhao, Y.; Wang, X.; Xu, H.; Guan, Y.; Jiang, J.; Song, W.; Han, Y.; Zhang, J.; Wu, P. Germanium-enriched double-four-membered-ring units inducing zeolite-confined subnanometric Pt clusters for efficient propane dehydrogenation. *Nature Catalysis* **2023**, *6* (6), 506−518.
(77) Sharma, S.; Maurer, F.; Lott, P.; Sheppard, T. L. Unlocking the Mysteries of Technical Catalyst Deactivation: A View from Space. *ChemCatChem.* **2024**, *16* (14), No. e202301655.
(78) Kumar, P.; Srivastava, V. C. Elucidation of Catalytic Propane Dehydrogenation Using Theoretical and Experimental Approaches: Advances and Outlook. *Energy Fuels* **2023**, *37* (23), 18369−18394.
(79) Sattler, J. J. H. B.; Mens, A. M.; Weckhuysen, B. M. Real-Time Quantitative Operando Raman Spectroscopy of a CrOx/Al2O3 Propane Dehydrogenation Catalyst in a Pilot-Scale Reactor. *ChemCatChem.* **2014**, *6* (11), 3139−3145.
(80) Wang, X.; Syed, Z. H.; Chen, Z.; Bazak, J. D.; Gong, X.; Wasson, M. C.; Washton, N. M.; Chapman, K. W.; Notestein, J. M.; Farha, O. K. Enhanced Catalytic Performance of a Ce/V Oxo Cluster through Confinement in Mesoporous SBA-15. *ACS Appl. Mater. Interfaces* **2022**, *14* (47), 52886−52893.
(81) Sharma, L.; Purdy, S. C.; Page, K.; Rangarajan, S.; Pham, H.; Datye, A.; Baltrusaitis, J. Sulfur Tolerant Subnanometer Fe/Alumina Catalysts for Propane Dehydrogenation. *ACS Applied Nano Materials* **2021**, *4* (10), 10055−10067.
(82) Matam, S. K.; Moffat, C.; Hellier, P.; Bowker, M.; Silverwood, I. P.; Catlow, C. R. A.; Jackson, S. D.; Craswell, J.; Wells, P. P.; Parker, S. F.; Gibson, E. K. Investigation of MoOx/Al2O3 under Cyclic Operation for Oxidative and Non-Oxidative Dehydrogenation of Propane. *Catalysts* **2020**, *10* (12), 1370.
(83) Lin, L.; Fan, M.; Sheveleva, A. M.; Han, X.; Tang, Z.; Carter, J. H.; da Silva, I.; Parlett, C. M. A.; Tuna, F.; McInnes, E. J. L.; Sastre, G.; Rudić, S.; Cavaye, H.; Parker, S. F.; Cheng, Y.; Daemen, L. L.; Ramirez-Cuesta, A. J.; Attfield, M. P.; Liu, Y.; Tang, C. C.; Han, B.; Yang, S. Control of zeolite microenvironment for propene synthesis from methanol. *Nat. Commun.* **2021**, *12* (1), 822.
(84) Hawkins, A. P.; Zachariou, A.; Parker, S. F.; Collier, P.; Silverwood, I. P.; Howe, R. F.; Lennon, D. Onset of Propene Oligomerization Reactivity in ZSM-5 Studied by Inelastic Neutron Scattering Spectroscopy. *ACS Omega* **2020**, *5* (14), 7762−7770.
(85) Becher, J.; Sanchez, D. F.; Doronkin, D. E.; Zengel, D.; Meira, D. M.; Pascarelli, S.; Grunwaldt, J.-D.; Sheppard, T. L. Chemical gradients

https://doi.org/10.1021/jacsau.4c00730
JACS Au 2024, 4, 4084−4109

in automotive Cu-SSZ-13 catalysts for NOx removal revealed by operando X-ray spectrotomography. *Nature Catalysis* **2021**, *4* (1), 46−53.
(86) Sheppard, T. L.; Price, S. W. T.; Benzi, F.; Baier, S.; Klumpp, M.; Dittmeyer, R.; Schwieger, W.; Grunwaldt, J.-D. In Situ Multimodal 3D Chemical Imaging of a Hierarchically Structured Core@Shell Catalyst. *J. Am. Chem. Soc.* **2017**, *139* (23), 7855−7863.
(87) Kang, J.; Carnis, J.; Kim, D.; Chung, M.; Kim, J.; Yun, K.; An, G.; Cha, W.; Harder, R.; Song, S.; Sikorski, M.; Robert, A.; Thanh, N. H.; Lee, H.; Choi, Y. N.; Huang, X.; Chu, Y. S.; Clark, J. N.; Song, M. K.; Yoon, K. B.; Robinson, I. K.; Kim, H. Time-resolved in situ visualization of the structural response of zeolites during catalysis. *Nat. Commun.* **2020**, *11* (1), 5901.
(88) Carl, S.; Will, J.; Madubuko, N.; Götz, A.; Przybilla, T.; Wu, M.; Raman, N.; Wirth, J.; Taccardi, N.; Zubiri, B. A.; Haumann, M.; Wasserscheid, P.; Spiecker, E. Structural Evolution of GaOx-Shell and Intermetallic Phases in Ga-Pt Supported Catalytically Active Liquid Metal Solutions. *J. Phys. Chem. Lett.* **2024**, *15* (17), 4711−4720.
(89) Dou, X.; Li, K.; Zhang, K.; Zhu, C.; Meira, D. M.; Song, Y.; He, P.; Zhang, L.; Liu, L. Isolated Pt Atoms Stabilized by Ga2O3 Clusters Confined in ZSM-5 for Nonoxidative Activation of Ethane. *JACS Au* **2024**, *4* (9), 3547−3557.
(90) Gan, Z.; Dewangan, N.; Wang, Z.; Liu, S.; Tan, X.; Kawi, S. Highly efficient and stable hydrogen permeable membrane reactor for propane dehydrogenation. *J. Membr. Sci.* **2024**, *701*, 122724.
(91) Li, C.; Wang, G. Dehydrogenation of light alkanes to mono-olefins. *Chem. Soc. Rev.* **2021**, *50* (7), 4359−4381.
(92) Amin, A. M.; Croiset, E.; Constantinou, C.; Epling, W. Methane cracking using Ni supported on porous and non-porous alumina catalysts. *Int. J. Hydrogen Energy* **2012**, *37* (11), 9038−9048.
(93) Boerefijn, R.; Gudde, N. J.; Ghadiri, M. A review of attrition of fluid cracking catalyst particles. *Advanced Powder Technology* **2000**, *11* (2), 145−174.
(94) Hao, J.; Zhao, Y.; Ye, M.; Liu, Z. Attrition of methanol to olefins catalyst with high-velocity air jets at elevated temperature. *Advanced Powder Technology* **2015**, *26* (3), 734−741.
(95) Wu, D.; Wu, F.; Li, Y. Particle size effect on the catalyst attrition in a lab-scale fluidized bed. *AIChE J.* **2017**, *63* (3), 914−920.
(96) Chiranjeevi, T.; Ravichander, N.; Gokak, D. T.; Ravikumar, V.; Choudary, N. V. The Selection of Fluid Catalytic Cracking Catalysts and Additives: The Significance of Attrition Studies. *Petroleum Science and Technology* **2014**, *32* (4), 470−478.
(97) Jager, B.; Espinoza, R. Advances in low temperature Fischer−Tropsch synthesis. *Catal. Today* **1995**, *23* (1), 17−28.
(98) Wang, G.; Yin, C.; Feng, F.; Zhang, Q.; Fu, H.; Bing, L.; Wang, F.; Han, D. Recent Progress on Catalyst Supports for Propane Dehydrogenation. *Current Nanoscience* **2023**, *19* (4), 473−483.
(99) Llorca, J.; Homs, N.; León, J.; Sales, J.; Fierro, J. L. G.; Ramirez de la Piscina, P. Supported Pt-Sn catalysts highly selective for isobutane dehydrogenation: preparation, characterization and catalytic behavior. *Applied Catalysis A: General* **1999**, *189* (1), 77−86.
(100) Xie, Y.; Kocaefe, D.; Kocaefe, Y.; Cheng, J.; Liu, W. The Effect of Novel Synthetic Methods and Parameters Control on Morphology of Nano-alumina Particles. *Nanoscale Res. Lett.* **2016**, *11* (1), 259.
(101) Shi, Y.; Li, X.; Rong, X.; Gu, B.; Wei, H.; Sun, C. Influence of support on the catalytic properties of Pt-Sn-K/θ-Al2O3 for propane dehydrogenation. *RSC Adv.* **2017**, *7* (32), 19841−19848.
(102) Liu, J.; Liu, C.; Ma, A.; Rong, J.; Da, Z.; Zheng, A.; Qin, L. Effects of Al2O3 phase and Cl component on dehydrogenation of propane. *Appl. Surf. Sci.* **2016**, *368*, 233−240.
(103) Kovarik, L.; Bowden, M.; Szanyi, J. High temperature transition aluminas in δ-Al2O3/θ-Al2O3 stability range: Review. *J. Catal.* **2021**, *393*, 357−368.
(104) Kwak, J. H.; Hu, J.; Lukaski, A.; Kim, D. H.; Szanyi, J.; Peden, C. H. F. Role of Pentacoordinated Al3+ Ions in the High Temperature Phase Transformation of γ-Al2O3. *J. Phys. Chem. C* **2008**, *112* (25), 9486−9492.
(105) Lu, J.; Liu, S.; Deng, C. Facile synthesis of alumina hollow spheres for on-plate-selective enrichment of phosphopeptides. *Chem. Commun.* **2011**, *47* (18), 5334−5336.
(106) Dai, Y.; Gu, J.; Tian, S.; Wu, Y.; Chen, J.; Li, F.; Du, Y.; Peng, L.; Ding, W.; Yang, Y. γ-Al2O3 sheet-stabilized isolate Co2+ for catalytic propane dehydrogenation. *J. Catal.* **2020**, *381*, 482−492.
(107) Li, L.; Liu, X.; Wang, G.; Liu, Y.; Kang, W.; Deng, N.; Zhuang, X.; Zhou, X. Research progress of ultrafine alumina fiber prepared by sol-gel method: A review. *Chemical Engineering Journal* **2021**, *421*, 127744.
(108) Shi, L.; Deng, G. M.; Li, W. C.; Miao, S.; Wang, Q. N.; Zhang, W. P.; Lu, A. H. Al2O3 nanosheets rich in pentacoordinate Al3+ ions stabilize Pt-Sn clusters for propane dehydrogenation. *Angew. Chem., Int. Ed.* **2015**, *54* (47), 13994−13998.
(109) Gong, N.; Zhao, Z. Peony-like Pentahedral Al(III)-Enriched Alumina Nanosheets for the Dehydrogenation of Propane. *ACS Applied Nano Materials* **2019**, *2* (9), 5833−5840.
(110) Huang, T.; Yu, Z.; Wang, Y.; Luo, G. Preparation of ultra-high-strength alumina microspheres based on fiber reconstruction via multistage low-carbon alcohol elution. *Powder Technol.* **2024**, *441*, 119833.
(111) Xu, J.; Ibrahim, A.-R.; Hu, X.; Hong, Y.; Su, Y.; Wang, H.; Li, J. Preparation of large pore volume γ-alumina and its performance as catalyst support in phenol hydroxylation. *Microporous Mesoporous Mater.* **2016**, *231*, 1−8.
(112) Rahmati, M.; Huang, B.; Mortensen, M. K.; Keyvanloo, K.; Fletcher, T. H.; Woodfield, B. F.; Hecker, W. C.; Argyle, M. D. Effect of different alumina supports on performance of cobalt Fischer−Tropsch catalysts. *J. Catal.* **2018**, *359*, 92−100.
(113) Zhang, Y.; Huang, B.; Mardkhe, M. K.; Woodfield, B. F. Thermal and hydrothermal stability of pure and silica-doped mesoporous aluminas. *Microporous Mesoporous Mater.* **2019**, *284*, 60−68.
(114) Yang, Y.; Miao, C.; Wang, R.; Zhang, R.; Li, X.; Wang, J.; Wang, X.; Yao, J. Advances in morphology-controlled alumina and its supported Pd catalysts: synthesis and applications. *Chem. Soc. Rev.* **2024**, *53* (10), 5014−5053.
(115) AbdelDayem, H. M.; Salib, B. G.; El-Hosiny, F. I. Facile synthesis of hydrothermal stable hierarchically macro-mesoporous hollow microspheres γ-Al2O3-graphene oxide composite: As a new efficient acid-base catalyst for transesterification reaction for biodiesel production. *Fuel* **2020**, *277*, 118106.
(116) Yang, Y.; Xu, Y.; Han, B.; Xu, B.; Liu, X.; Yan, Z. Effects of synthetic conditions on the textural structure of pseudo-boehmite. *J. Colloid Interface Sci.* **2016**, *469*, 1−7.
(117) Zhao, Z.; Yang, J.; Xu, N.; Nan, T.; Wu, P.; Wang, C.; Wang, X.; Bai, P.; Yan, Z.; Mintova, S. Generation and nature of water-tolerant Lewis acid sites in InxSn10-xOy/Al2O3 catalysts as active centers for the green synthesis of methyl lactate from glucose. *Inorganic Chemistry Frontiers* **2023**, *10* (5), 1574−1586.
(118) Liu, C.; Li, R.; Wang, F.; Li, K.; Fan, Y.; Mu, R.; Fu, Q. Water promoted structural evolution of Ag nanocatalysts supported on alumina. *Nano Research* **2023**, *16* (7), 9107−9115.
(119) Fan, Y.; Wang, F.; Li, R.; Liu, C.; Fu, Q. Surface Hydroxyl-Determined Migration and Anchoring of Silver on Alumina in Oxidative Redispersion. *ACS Catal.* **2023**, *13* (4), 2277−2285.
(120) Su, N.; Mu, R.; Wu, H.; Zhang, R.; Zhao, S.; Li, Y.; Fu, Q.; Bao, X. Active sites for H2 and H2O activation over bifunctional ZnO-Pt(1 1 1) model catalysts. *Appl. Surf. Sci.* **2020**, *503*, 144204.
(121) Wang, D.; Li, R.; Sun, X.; Lin, L.; Li, K.; Zhang, R.; Mu, R.; Fu, Q. Hydroxide Structure-Dependent OH Promotion Mechanism over a Hydroxylated CoOx/Pt(111) Catalyst toward CO Oxidation. *ACS Catal.* **2024**, *14* (7), 5147−5155.
(122) Aitbekova, A.; Zhou, C.; Stone, M. L.; Lezama-Pacheco, J. S.; Yang, A.-C.; Hoffman, A. S.; Goodman, E. D.; Huber, P.; Stebbins, J. F.; Bustillo, K. C.; Ercius, P.; Ciston, J.; Bare, S. R.; Plessow, P. N.; Cargnello, M. Templated encapsulation of platinum-based catalysts promotes high-temperature stability to 1,100 °C. *Nat. Mater.* **2022**, *21* (11), 1290−1297.

https://doi.org/10.1021/jacsau.4c00730
JACS Au 2024, 4, 4084−4109

(123) Bara, C.; Plais, L.; Larmier, K.; Devers, E.; Digne, M.; Lamic-Humblot, A.-F.; Pirngruber, G. D.; Carrier, X. Aqueous-Phase Preparation of Model HDS Catalysts on Planar Alumina Substrates: Support Effect on Mo Adsorption and Sulfidation. *J. Am. Chem. Soc.* **2015**, *137* (50), 15915−15928.
(124) Bazyari, A.; Mortazavi, Y.; Khodadadi, A. A.; Thompson, L. T.; Tafreshi, R.; Zaker, A.; Ajenifujah, O. T. Effects of alumina phases as nickel supports on deep reactive adsorption of (4,6-dimethyl) dibenzothiophene: Comparison between γ, δ, and θ-alumina. *Applied Catalysis B: Environmental* **2016**, *180*, 312−323.
(125) Lee, J.; Jeon, H.; Oh, D. G.; Szanyi, J.; Kwak, J. H. Morphology-dependent phase transformation of γ-Al2O3. *Applied Catalysis A: General* **2015**, *500*, 58−68.
(126) Morgan, K.; Goguet, A.; Hardacre, C. Metal Redispersion Strategies for Recycling of Supported Metal Catalysts: A Perspective. *ACS Catal.* **2015**, *5* (6), 3430−3445.
(127) Simancas, R.; Chokkalingam, A.; Elangovan, S. P.; Liu, Z.; Sano, T.; Iyoki, K.; Wakihara, T.; Okubo, T. Recent progress in the improvement of hydrothermal stability of zeolites. *Chemical Science* **2021**, *12* (22), 7677−7695.
(128) Huo, J.; Tessonnier, J.-P.; Shanks, B. H. Improving Hydrothermal Stability of Supported Metal Catalysts for Biomass Conversions: A Review. *ACS Catal.* **2021**, *11* (9), 5248−5270.
(129) Camblor, M. A.; Villaescusa, L. A.; Díaz-Cabañas, M. J. Synthesis of all-silica and high-silica molecular sieves in fluoride media. *Top. Catal.* **1999**, *9* (1), 59−76.
(130) Moteki, T.; Lobo, R. F. A General Method for Aluminum Incorporation into High-Silica Zeolites Prepared in Fluoride Media. *Chem. Mater.* **2016**, *28* (2), 638−649.
(131) Akiyama, S.; Mochizuki, H.; Yamazaki, H.; Yokoi, T.; Tatsumi, T.; Kondo, J. N. The effective silylation of external surface on H-ZSM5 with cyclic siloxane for the catalytic cracking of naphtha. *Molecular Catalysis* **2017**, *433*, 48−54.
(132) Zhu, Z.; Xie, Z.; Chen, Q.; Kong, D.; Li, W.; Yang, W.; Li, C. Chemical liquid deposition with polysiloxane of ZSM-5 and its effect on acidity and catalytic properties. *Microporous Mesoporous Mater.* **2007**, *101* (1), 169−175.
(133) Prodinger, S.; Derewinski, M. A.; Vjunov, A.; Burton, S. D.; Arslan, I.; Lercher, J. A. Improving Stability of Zeolites in Aqueous Phase via Selective Removal of Structural Defects. *J. Am. Chem. Soc.* **2016**, *138* (13), 4408−4415.
(134) Martínez, C.; Verboekend, D.; Pérez-Ramírez, J.; Corma, A. Stabilized hierarchical USY zeolite catalysts for simultaneous increase in diesel and LPG olefinicity during catalytic cracking. *Catalysis Science & Technology* **2013**, *3* (4), 972−981.
(135) Sousa-Aguiar, E. F.; Trigueiro, F. E.; Zotin, F. M. Z. The role of rare earth elements in zeolites and cracking catalysts. *Catal. Today* **2013**, *218−219*, 115−122.
(136) Blay, V.; Louis, B.; Miravalles, R.; Yokoi, T.; Peccatiello, K. A.; Clough, M.; Yilmaz, B. Engineering Zeolites for Catalytic Cracking to Light Olefins. *ACS Catal.* **2017**, *7* (10), 6542−6566.
(137) Blasco, T.; Corma, A.; Martínez-Triguero, J. Hydrothermal stabilization of ZSM-5 catalytic-cracking additives by phosphorus addition. *J. Catal.* **2006**, *237* (2), 267−277.
(138) Lercher, J. A.; Rumplmayr, G. Controlled decrease of acid strength by orthophosphoric acid on ZSM5. *Applied Catalysis* **1986**, *25* (1), 215−222.
(139) Chu, Y.; Gao, X.; Zhang, X.; Xu, G.; Li, G.; Zheng, A. Identifying the effective phosphorous species over modified P-ZSM-5 zeolite: a theoretical study. *Phys. Chem. Chem. Phys.* **2018**, *20* (17), 11702−11712.
(140) Arteaga, G. J.; Anderson, J. A.; Rochester, C. H. Effects of Oxidation-Reduction and Oxychlorination-Reduction Cycles on CO Adsorption by Pt-Sn/Al2O3Catalysts. *J. Catal.* **1999**, *184* (1), 268−279.
(141) Weller, S. W.; Montagna, A. A. O2 chemisorption at high temperatures on platinum-alumina and platinum-zeolite. *J. Catal.* **1971**, *20* (3), 394−407.
(142) Newton, M. A.; Belver-Coldeira, C.; Martínez-Arias, A.; Fernández-García, M. Dynamic in situ observation of rapid size and shape change of supported Pd nanoparticles during CO/NO cycling. *Nat. Mater.* **2007**, *6* (7), 528−532.
(143) Newton, M. A.; Belver-Coldeira, C.; Martínez-Arias, A.; Fernández-García, M. Oxidationless" Promotion of Rapid Palladium Redispersion by Oxygen during Redox CO/(NO+O2) Cycling. *Angew. Chem., Int. Ed.* **2007**, *46* (45), 8629−8631.
(144) Nishihata, Y.; Mizuki, J.; Akao, T.; Tanaka, H.; Uenishi, M.; Kimura, M.; Okamoto, T.; Hamada, N. Self-regeneration of a Pd-perovskite catalyst for automotive emissions control. *Nature* **2002**, *418* (6894), 164−167.
(145) Tanaka, H.; Taniguchi, M.; Uenishi, M.; Kajita, N.; Tan, I.; Nishihata, Y.; Mizuki, J. i.; Narita, K.; Kimura, M.; Kaneko, K. Self-Regenerating Rh- and Pt-Based Perovskite Catalysts for Automotive-Emissions Control. *Angew. Chem., Int. Ed.* **2006**, *45* (36), 5998−6002.
(146) Chong, F. K.; Anderson, J. A.; Rochester, C. H. Effects of regeneration cycles on heptane-H2 reactions over Pt-Re/Al2O3 catalysts. *Phys. Chem. Chem. Phys.* **2000**, *2* (24), 5730−5736.
(147) Breen, J. P.; Burch, R.; Hardacre, C.; Hill, C. J.; Krutzsch, B.; Bandl-Konrad, B.; Jobson, E.; Cider, L.; Blakeman, P. G.; Peace, L. J.; Twigg, M. V.; Preis, M.; Gottschling, M. An investigation of the thermal stability and sulphur tolerance of Ag/γ-Al2O3 catalysts for the SCR of NOx with hydrocarbons and hydrogen. *Applied Catalysis B: Environmental* **2007**, *70* (1), 36−44.
(148) Bernal, S.; Calvino, J. J.; Cauqui, M. A.; Pérez Omil, J. A.; Pintado, J. M.; Rodrıguez-Izquierdo, J. M. Image simulation and experimental HREM study of the metal dispersion in Rh/CeO2 catalysts. Influence of the reduction/reoxidation conditions. *Applied Catalysis B: Environmental* **1998**, *16* (2), 127−138.
(149) Lai, X. P.; St.Clair, T.; Wayne Goodman, D. Oxygen-induced morphological changes of Ag nanoclusters supported on TiO2(110). *Faraday Discuss.* **1999**, *114* (0), 279−284.
(150) Baker, R. T. K.; Thomas, C.; Thomas, R. B. Continuous observation of the particle size behavior of platinum on alumina. *J. Catal.* **1975**, *38* (1), 510−513.
(151) Kartusch, C.; Krumeich, F.; Safonova, O.; Hartfelder, U.; Makosch, M.; Sá, J.; van Bokhoven, J. A. Redispersion of Gold Multiple-Twinned Particles during Liquid-Phase Hydrogenation. *ACS Catal.* **2012**, *2* (7), 1394−1403.
(152) Ruckenstein, E.; Malhotra, M. L. Splitting of platinum crystallites supported on thin, nonporous alumina films. *J. Catal.* **1976**, *41* (2), 303−311.
(153) Fiedorow, R. M.; Wanke, S. E. The sintering of supported metal catalysts: I. Redispersion of supported platinum in oxygen. *J. Catal.* **1976**, *43* (1−3), 34−42.
(154) Campbell, C. T.; Mao, Z. Chemical Potential of Metal Atoms in Supported Nanoparticles: Dependence upon Particle Size and Support. *ACS Catal.* **2017**, *7* (12), 8460−8466.
(155) Pham, H. N.; Sattler, J. J. H. B.; Weckhuysen, B. M.; Datye, A. K. Role of Sn in the Regeneration of Pt/γ-Al2O3 Light Alkane Dehydrogenation Catalysts. *ACS Catal.* **2016**, *6* (4), 2257−2264.
(156) Moliner, M.; Gabay, J.; Kliewer, C.; Serna, P.; Corma, A. Trapping of Metal Atoms and Metal Clusters by Chabazite under Severe Redox Stress. *ACS Catal.* **2018**, *8* (10), 9520−9528.
(157) Felvey, N.; Guo, J.; Rana, R.; Xu, L.; Bare, S. R.; Gates, B. C.; Katz, A.; Kulkarni, A. R.; Runnebaum, R. C.; Kronawitter, C. X. Interconversion of Atomically Dispersed Platinum Cations and Platinum Clusters in Zeolite ZSM-5 and Formation of Platinum gem-Dicarbonyls. *J. Am. Chem. Soc.* **2022**, *144* (30), 13874−13887.
(158) Adamiec, J.; Fiedorow, R. M.; Wanke, S. E. The influence of acid-base properties of oxide supports on platinum dispersion during oxygen treatments. *J. Catal.* **1985**, *95* (2), 492−500.
(159) Baker, R.; Thomas, C.; Thomas, R. Continuous observation of the particle size behavior of platinum on alumina. *Journal of catalysis* **1975**, *38* (1−3), 510−513.
(160) Lieske, H.; Lietz, G.; Spindler, H.; Völter, J. Reactions of platinum in oxygen-and hydrogen-treated Ptγ-Al2O3 catalysts: I.

https://doi.org/10.1021/jacsau.4c00730
JACS Au 2024, 4, 4084−4109

Temperature-programmed reduction, adsorption, and redispersion of platinum. *Journal of catalysis* **1983**, *81* (1), 8−16.
(161) Lietz, G.; Lieske, H.; Spindler, H.; Hanke, W.; Völter, J. Reactions of platinum in oxygen-and hydrogen-treated Ptγ-Al2O3 catalysts: II. Ultraviolet-visible studies, sintering of platinum, and soluble platinum. *J. Catal.* **1983**, *81* (1), 17−25.
(162) Mordente, M. G. V.; Rochester, C. H. Infrared study of the effects of oxychlorination on Pt dispersion in Pt/Al2O3 catalysts. *Journal of the Chemical Society, Faraday Transactions 1: Physical Chemistry in Condensed Phases* **1989**, *85* (10), 3495−3504.
(163) Le Normand, F.; Borgna, A.; Garetto, T. F.; Apesteguia, C. R.; Moraweck, B. Redispersion of sintered Pt/Al2O3 naphtha reforming catalysts: An in situ study monitored by X-ray absorption spectroscopy. *J. Phys. Chem.* **1996**, *100* (21), 9068−9076.
(164) Hung, C.-C.; Yeh, C.-Y.; Shih, C.-C.; Chang, J.-R. Oxychlorination Redispersion of Pt Catalysts: Surface Species and Pt-Support Interactions Characterized by X-ray Absorption and FT-IR Spectroscopy. *Catalysts* **2019**, *9* (4), 362.
(165) Foger, K.; Jaeger, H. Redispersion of Pt—zeolite catalysts with chlorine. *Applied Catalysis* **1989**, *56* (1), 137−147.
(166) Foger, K.; Jaeger, H. The effect of chlorine treatment on the dispersion of platinum metal particles supported on silica and γ-alumina. *J. Catal.* **1985**, *92* (1), 64−78.
(167) Foger, K.; Hay, D.; Jaeger, H. The redispersion of iridium on SiO2 and γ-Al2O3 supports with chlorine-containing gases. *J. Catal.* **1985**, *96* (1), 154−169.
(168) Ren, G.; Xiong, S.; Li, X.; Lai, X.; Chen, J.; Chu, M.; Xu, Y.; Huang, S. Regeneration of sintered platinum at mild temperature for propane dehydrogenation. *J. Catal.* **2024**, *429*, 115276.
(169) Dorling, T.; Moss, R. The structure and activity of supported metal catalysts: I. Crystallite size and specific activity for benzene hydrogenation of platinum/silica catalysts. *J. Catal.* **1966**, *5* (1), 111−115.
(170) Akhtar, M. N.; Aitani, A. M.; Ummer, A. C.; Alasiri, H. S. Review on the Catalytic Conversion of Naphtha to Aromatics: Advances and Outlook. *Energy Fuels* **2023**, *37* (4), 2586−2607.
(171) Matthew, P.; Mark, S. CATALYTIC DEHYDROGENATION PROCESS. AR098383A1, 05/26/2016.
(172) Pretz, M.; Fish, B. B.; Luo, L.; Stears, B. A. J. H. P. Shaping the future of on-purpose propylene production. *Hydrocarbon Processing* **2017**, *96*, 36.
(173) A. Maddah, H. A Comparative Study between Propane Dehydrogenation (PDH) Technologies and Plants in Saudi Arabia. *American Scientific Research Journal for Engineering, Technology, and Sciences* **2018**, *45* (1), 49−63.
(174) Pati, S.; Dewangan, N.; Jangam, A.; Kawi, S. Catalytic membrane reactors for alkane dehydrogenation applications: an integration of catalysis and separation process. *Reviews in Chemical Engineering* **2024**, *40* (3), 351−375.
(175) Yacob, S.; Caulfield, M.; Larson, R. B.; Gomez, E.; Meyer, R. J. The Interplay between Process Conceptualization and Experimental Research−Accelerating and Guiding Catalysis to Process Breakthroughs. *ACS Catal.* **2022**, *12* (17), 10621−10628.
(176) Sattler, A.; Paccagnini, M.; Gomez, E.; Meyer, R. J.; Yacob, S.; Klutse, H.; Caulfield, M.; Gao, Y. Catalytic limitations on alkane dehydrogenation under H2 deficient conditions relevant to membrane reactors. *Energy Environ. Sci.* **2022**, *15* (5), 2120−2129.
(177) Shelepova, E. V.; Vedyagin, A. A.; Mishakov, I. V.; Noskov, A. S. Simulation of hydrogen and propylene coproduction in catalytic membrane reactor. *Int. J. Hydrogen Energy* **2015**, *40* (8), 3592−3598.
(178) Chen, Y.-R.; Tsuru, T.; Kang, D.-Y. Simulation and design of catalytic membrane reactor for hydrogen production via methylcyclohexane dehydrogenation. *Int. J. Hydrogen Energy* **2017**, *42* (42), 26296−26307.
(179) Koutsonikolas, D.; Kaldis, S.; Zaspalis, V. T.; Sakellaropoulos, G. P. Potential application of a microporous silica membrane reactor for cyclohexane dehydrogenation. *Int. J. Hydrogen Energy* **2012**, *37* (21), 16302−16307.
(180) Li, G.; Yada, K.; Kanezashi, M.; Yoshioka, T.; Tsuru, T. Methylcyclohexane Dehydrogenation in Catalytic Membrane Reactors for Efficient Hydrogen Production. *Ind. Eng. Chem. Res.* **2013**, *52* (37), 13325−13332.
(181) Maneerung, T.; Hidajat, K.; Kawi, S. Ultra-thin (<1μm) internally-coated Pd-Ag alloy hollow fiber membrane with superior thermal stability and durability for high temperature H2 separation. *J. Membr. Sci.* **2014**, *452*, 127−142.
(182) Schäfer, R.; Noack, M.; Kölsch, P.; Thomas, S.; Seidel-Morgenstern, A.; Caro, J. Development of a H2-selective SiO2-membrane for the catalytic dehydrogenation of propane. *Sep. Purif. Technol.* **2001**, *25* (1), 3−9.
(183) Avila, A. M.; Yu, Z.; Fazli, S.; Sawada, J. A.; Kuznicki, S. M. Hydrogen-selective natural mordenite in a membrane reactor for ethane dehydrogenation. *Microporous Mesoporous Mater.* **2014**, *190*, 301−308.
(184) Wang, Z.; Li, Z.; Cui, Y.; Chen, T.; Hu, J.; Kawi, S. Highly Efficient NO Decomposition via Dual-Functional Catalytic Perovskite Hollow Fiber Membrane Reactor Coupled with Partial Oxidation of Methane at Medium-Low Temperature. *Environ. Sci. Technol.* **2019**, *53* (16), 9937−9946.
(185) Conde, J. J.; Maroño, M.; Sánchez-Hervás, J. M. Pd-Based Membranes for Hydrogen Separation: Review of Alloying Elements and Their Influence on Membrane Properties. *Separation & Purification Reviews* **2017**, *46* (2), 152−177.
(186) Tew, M. W.; Nachtegaal, M.; Janousch, M.; Huthwelker, T.; van Bokhoven, J. A. The irreversible formation of palladium carbide during hydrogenation of 1-pentyne over silica-supported palladium nanoparticles: in situ Pd K and L3 edge XAS. *Phys. Chem. Chem. Phys.* **2012**, *14* (16), 5761−5768.
(187) Peters, T. A.; Liron, O.; Tschentscher, R.; Sheintuch, M.; Bredesen, R. Investigation of Pd-based membranes in propane dehydrogenation (PDH) processes. *Chemical Engineering Journal* **2016**, *305*, 191−200.
(188) Mundschau, M. V.; Xie, X.; Evenson, C. R.; Sammells, A. F. Dense inorganic membranes for production of hydrogen from methane and coal with carbon dioxide sequestration. *Catal. Today* **2006**, *118* (1), 12−23.
(189) Ali, J. K.; Newson, E. J.; Rippin, D. W. T. Deactivation and regeneration of Pd═Ag membranes for dehydrogenation reactions. *J. Membr. Sci.* **1994**, *89* (1), 171−184.
(190) Morreale, B. D.; Ciocco, M. V.; Howard, B. H.; Killmeyer, R. P.; Cugini, A. V.; Enick, R. M. Effect of hydrogen-sulfide on the hydrogen permeance of palladium-copper alloys at elevated temperatures. *J. Membr. Sci.* **2004**, *241* (2), 219−224.
(191) Kulprathipanja, A.; Alptekin, G. O.; Falconer, J. L.; Way, J. D. Pd and Pd-Cu membranes: inhibition of H2 permeation by H2S. *J. Membr. Sci.* **2005**, *254* (1), 49−62.
(192) McKinley, D. L. Metal alloy for hydrogen separation and purification. US3350845A, 11/07/1967.
(193) Flanagan, T. B.; Wang, D. Hydrogen Permeation through fcc Pd-Au Alloy Membranes. *J. Phys. Chem. C* **2011**, *115* (23), 11618−11623.
(194) Sonwane, C. G.; Wilcox, J.; Ma, Y. H. Achieving optimum hydrogen permeability in PdAg and PdAu alloys. *J. Chem. Phys.* **2006**, *125* (18), 184714.
(195) Sabina, K. G.; Kent, E. C.; Douglas Way, J. Effects of fabrication technique upon material properties and permeation characteristics of palladium-gold alloy membranes for hydrogen separations. *Gold Bulletin* **2010**, *43* (4), 287−297.
(196) Løvvik, O. M.; Peters, T. A.; Bredesen, R. First-principles calculations on sulfur interacting with ternary Pd-Ag-transition metal alloy membrane alloys. *J. Membr. Sci.* **2014**, *453*, 525−531.
(197) Hong, M.; Li, S.; Falconer, J. L.; Noble, R. D. Hydrogen purification using a SAPO-34 membrane. *J. Membr. Sci.* **2008**, *307* (2), 277−283.
(198) Qi, H.; Han, J.; Xu, N.; Bouwmeester, H. J. Hybrid organic-inorganic microporous membranes with high hydrothermal stability for

https://doi.org/10.1021/jacsau.4c00730
JACS Au 2024, 4, 4084−4109

the separation of carbon dioxide. *ChemSusChem* **2010**, *3* (12), 1375−1378.
(199) ten Hove, M.; Luiten-Olieman, M. W.; Huiskes, C.; Nijmeijer, A.; Winnubst, L. Hydrothermal stability of silica, hybrid silica and Zr-doped hybrid silica membranes. *Sep. Purif. Technol.* **2017**, *189*, 48−53.
(200) Huang, A.; Dou, W.; Caro, J. r. Steam-stable zeolitic imidazolate framework ZIF-90 membrane with hydrogen selectivity through covalent functionalization. *J. Am. Chem. Soc.* **2010**, *132* (44), 15562−15564.
(201) Marković, A.; Stoltenberg, D.; Enke, D.; Schlünder, E.-U.; Seidel-Morgenstern, A. Gas permeation through porous glass membranes: Part II: Transition regime between Knudsen and configurational diffusion. *J. Membr. Sci.* **2009**, *336* (1−2), 32−41.
(202) Carreon, M. A.; Li, S.; Falconer, J. L.; Noble, R. D. Alumina-supported SAPO-34 membranes for CO2/CH4 separation. *J. Am. Chem. Soc.* **2008**, *130* (16), 5412−5413.
(203) Yu, M.; Funke, H. H.; Noble, R. D.; Falconer, J. L. H2 separation using defect-free, inorganic composite membranes. *J. Am. Chem. Soc.* **2011**, *133* (6), 1748−1750.
(204) Liu, L.; Bhowmick, A.; Cheng, S.; Blazquez, B. H.; Pan, Y.; Zhang, J.; Zhang, Y.; Shu, Y.; Tran, D. T.; Luo, Y.; Ierapetritou, M.; Zhang, C.; Liu, D. Alkane dehydrogenation in scalable and electrifiable carbon membrane reactor. *Cell Reports Physical Science* **2023**, *4* (12), 101692.
(205) Zhou, J.; Zhao, J.; Zhang, J.; Zhang, T.; Ye, M.; Liu, Z. Regeneration of catalysts deactivated by coke deposition: A review. *Chinese Journal of Catalysis* **2020**, *41* (7), 1048−1061.
(206) Paglieri, S.; Way, J. Innovations in palladium membrane research. *Separation and Purification Methods* **2002**, *31* (1), 1−169.
(207) Pati, S.; Dewangan, N.; Wang, Z.; Jangam, A.; Kawi, S. Nanoporous zeolite-A sheltered Pd-hollow fiber catalytic membrane reactor for propane dehydrogenation. *ACS Applied Nano Materials* **2020**, *3* (7), 6675−6683.
(208) Abate, S.; Diaz, U.; Prieto, A.; Gentiluomo, S.; Palomino, M.; Perathoner, S.; Corma, A.; Centi, G. Influence of zeolite protective overlayer on the performances of Pd thin film membrane on tubular asymmetric alumina supports. *Ind. Eng. Chem. Res.* **2016**, *55* (17), 4948−4959.
(209) Yu, J.; Qi, C.; Zhang, J.; Bao, C.; Xu, H. Synthesis of a zeolite membrane as a protective layer on a metallic Pd composite membrane for hydrogen purification. *Journal of Materials Chemistry A* **2015**, *3* (9), 5000−5006.
(210) Huang, Y.; Shu, S.; Lu, Z.; Fan, Y. Characterization of the adhesion of thin palladium membranes supported on tubular porous ceramics. *Thin Solid Films* **2007**, *515* (13), 5233−5240.
(211) Okazaki, J.; Ikeda, T.; Pacheco Tanaka, D. A.; Llosa Tanco, M. A.; Wakui, Y.; Sato, K.; Mizukami, F.; Suzuki, T. M. Importance of the support material in thin palladium composite membranes for steady hydrogen permeation at elevated temperatures. *Phys. Chem. Chem. Phys.* **2009**, *11*, 8632−8638.
(212) Okazaki, J.; Ikeda, T.; Tanaka, D. A. P.; Sato, K.; Suzuki, T. M.; Mizukami, F. An investigation of thermal stability of thin palladium-silver alloy membranes for high temperature hydrogen separation. *J. Membr. Sci.* **2011**, *366* (1−2), 212−219.
(213) Kim, S.-J.; Liu, Y.; Moore, J. S.; Dixit, R. S.; Pendergast, J. G., Jr; Sholl, D.; Jones, C. W.; Nair, S. Thin hydrogen-selective SAPO-34 zeolite membranes for enhanced conversion and selectivity in propane dehydrogenation membrane reactors. *Chem. Mater.* **2016**, *28* (12), 4397−4402.
(214) Kim, S.-J.; Tan, S.; Taborga Claure, M.; Briones Gil, L.; More, K. L.; Liu, Y.; Moore, J. S.; Dixit, R. S.; Pendergast, J. G., Jr; Sholl, D. S.; et al. One-step synthesis of zeolite membranes containing catalytic metal nanoclusters. *ACS Applied Materials Interfaces* **2016**, *8* (37), 24671−24681.
(215) Almallahi, R.; Wortman, J.; Linic, S. Overcoming limitations in propane dehydrogenation by codesigning catalyst-membrane systems. *Science* **2024**, *383* (6689), 1325−1331.
(216) Wang, P.; Zhang, X.; Shi, R.; Zhao, J.; Waterhouse, G. I. N.; Tang, J.; Zhang, T. Photocatalytic ethylene production by oxidative dehydrogenation of ethane with dioxygen on ZnO-supported PdZn intermetallic nanoparticles. *Nat. Commun.* **2024**, *15* (1), 789.
(217) Wang, X.; Pei, C.; Zhao, Z.-J.; Chen, S.; Li, X.; Sun, J.; Song, H.; Sun, G.; Wang, W.; Chang, X.; Zhang, X.; Gong, J. Coupling acid catalysis and selective oxidation over MoO3-Fe2O3 for chemical looping oxidative dehydrogenation of propane. *Nat. Commun.* **2023**, *14* (1), 2039.
(218) Chen, S.; Luo, R.; Zhao, Z.-J.; Pei, C.; Xu, Y.; Lu, Z.; Zhao, C.; Song, H.; Gong, J. Concerted oxygen diffusion across heterogeneous oxide interfaces for intensified propane dehydrogenation. *Nat. Commun.* **2023**, *14* (1), 2620.
(219) Grasselli, R. K.; Stern, D. L.; Tsikoyiannis, J. G. Catalytic dehydrogenation (DH) of light paraffins combined with selective hydrogen combustion (SHC): II. DH+SHC catalysts physically mixed (redox process mode). *Applied Catalysis A: General* **1999**, *189* (1), 9−14.
(220) Låte, L.; Thelin, W.; Blekkan, E. A. Selective combustion of hydrogen in the presence of hydrocarbons: Part 2. Metal oxide based catalysts. *Applied Catalysis A: General* **2004**, *262* (1), 63−68.
(221) Tsikoyiannis, J. G.; Stern, D. L.; Grasselli, R. K. Metal Oxides As Selective Hydrogen Combustion (SHC) Catalysts and Their Potential in Light Paraffin Dehydrogenation. *J. Catal.* **1999**, *184* (1), 77−86.
(222) Kim, S.; Annamalai, L.; Lobo, R. F. Silica-encapsulated Fe2O3 oxygen carriers for selective chemical looping combustion of hydrogen. *Chemical Engineering Journal* **2023**, *455*, 140919.
(223) Dudek, R. B.; Li, F. Selective hydrogen combustion as an effective approach for intensified chemical production via the chemical looping strategy. *Fuel Process. Technol.* **2021**, *218*, 106827.
(224) Rothenberg, G.; de Graaf, E. A.; Bliek, A. Solvent-Free Synthesis of Rechargeable Solid Oxygen Reservoirs for Clean Hydrogen Oxidation. *Angew. Chem., Int. Ed.* **2003**, *42* (29), 3366−3368.
(225) Li, F.; Wang, B.; Chen, X.; Lai, Y.; Wang, T.; Fan, H.; Yang, X.; Guo, Q. Photocatalytic Oxidative Dehydrogenation of Propane for Selective Propene Production with TiO2. *JACS Au* **2022**, *2* (11), 2607−2616.
(226) Hu, Z.; Zhu, J.; Chen, R.; Wu, Y.; Zheng, K.; Liu, C.; Pan, Y.; Chen, J.; Sun, Y.; Xie, Y. High-Rate and Selective C2H6-to-C2H4 Photodehydrogenation Enabled by Partially Oxidized Pdδ+ Species Anchored on ZnO Nanosheets under Mild Conditions. *J. Am. Chem. Soc.* **2024**, *146* (24), 16490−16498.
(227) Zhang, L.; Liu, L.; Pan, Z.; Zhang, R.; Gao, Z.; Wang, G.; Huang, K.; Mu, X.; Bai, F.; Wang, Y.; Zhang, W.; Cui, Z.; Li, L. Visible-light-driven non-oxidative dehydrogenation of alkanes at ambient conditions. *Nature Energy* **2022**, *7* (11), 1042−1051.
(228) He, Z.-H.; Wu, B.-T.; Wang, Z.-Y.; Yang, S.-Y.; Wang, K.; Shi, J.-J.; He, M.-X.; Wang, W.; Liu, Z.-T. Photothermal catalytic CO2 oxidative dehydrogenation of propane to propylene over BiOX (X = Cl, Br, I) nanocatalysts. *Green Chem.* **2022**, *24* (21), 8270−8279.
(229) Zhu, Z.-J.; He, Z.-H.; Wang, S.-W.; Wu, B.-T.; Tian, Y.; Sun, Y.-C.; Wang, K.; Wang, W.; Wang, H.; Liu, Z.-T. Photothermal catalytic CO2 oxidative dehydrogenation of propane over Co-Mn bimetallic oxides supported on MCM-41 molecular sieve. *Molecular Catalysis* **2024**, *559*, 114070.
(230) Yang, D.; Liu, D.; Li, Y.; Gan, H.; Xu, P.; Tian, Y.; Li, Z.; Xing, T.; Gu, X.; Li, L.; Wang, X.; Wei, L.; Dai, P.; Wu, M. Photo-thermal synergistic catalytic oxidative dehydrogenation of propane over a spherical superstructure of boron carbon nitride nanosheets. *Appl. Surf. Sci.* **2023**, *639*, 158258.
(231) Koshti, H.; Bandyopadhyay, M.; Kumar, M.; Tsunoji, N.; Bandyopadhyay, R. Alkylation of Toluene to Mono-benzylated Toluene over Micro-mesoporous Zeolite: Effect of Post-synthetic Treatment and Catalytic Application. *Eur. J. Inorg. Chem.* **2023**, *27* (5), No. e202300674.
(232) Ji, X.; Ma, Y.; Sun, X.; Song, S.; Yang, K.; Huang, W.; Xu, C.; Feng, B.; Liu, J.; Song, W. Photothermal Propane Dehydrogenation Catalyzed by VOx-Doped TiO2 Nanoparticles. *ACS Applied Nano Materials* **2023**, *6* (7), 6354−6364.

https://doi.org/10.1021/jacsau.4c00730
JACS Au 2024, 4, 4084−4109

(233) Song, C.; Wang, Z.; Yin, Z.; Xiao, D.; Ma, D. Principles and applications of photothermal catalysis. *Chem. Catalysis* **2022**, *2* (1), 52−83.
(234) Cai, M.; Li, C.; An, X.; Zhong, B.; Zhou, Y.; Feng, K.; Wang, S.; Zhang, C.; Xiao, M.; Wu, Z.; He, J.; Wu, C.; Shen, J.; Zhu, Z.; Feng, K.; Zhong, J.; He, L. Supra-Photothermal CO2Methanation over Greenhouse-Like Plasmonic Superstructures of Ultrasmall Cobalt Nanoparticles. *Adv. Mater.* **2024**, *36* (9), 2308859.
(235) Li, X.; Li, L.; Chu, X.; Liu, X.; Chen, G.; Guo, Q.; Zhang, Z.; Wang, M.; Wang, S.; Tahn, A.; Sun, Y.; Feng, X. Photothermal CO2 conversion to ethanol through photothermal heterojunction-nanosheet arrays. *Nat. Commun.* **2024**, *15* (1), 5639.
(236) Cai, M.; Wu, Z.; Li, Z.; Wang, L.; Sun, W.; Tountas, A. A.; Li, C.; Wang, S.; Feng, K.; Xu, A.-B.; Tang, S.; Tavasoli, A.; Peng, M.; Liu, W.; Helmy, A. S.; He, L.; Ozin, G. A.; Zhang, X. Greenhouse-inspired supra-photothermal CO2 catalysis. *Nature Energy* **2021**, *6* (8), 807−814.
(237) Hong, J.; Xu, C.; Deng, B.; Gao, Y.; Zhu, X.; Zhang, X.; Zhang, Y. Photothermal Chemistry Based on Solar Energy: From Synergistic Effects to Practical Applications. *Advanced Science* **2022**, *9* (3), 2103926.
(238) Zhang, J.; Chen, H.; Duan, X.; Sun, H.; Wang, S. Photothermal catalysis: From fundamentals to practical applications. *Mater. Today* **2023**, *68*, 234−253.
(239) Kwak, Y.; Wang, C.; Kavale, C. A.; Yu, K.; Selvam, E.; Mallada, R.; Santamaria, J.; Julian, I.; Catala-Civera, J. M.; Goyal, H.; Zheng, W.; Vlachos, D. G. Microwave-assisted, performance-advantaged electrification of propane dehydrogenation. *Science Advances* **2023**, *9* (37), No. eadi8219.
(240) Haneishi, N.; Tsubaki, S.; Abe, E.; Maitani, M. M.; Suzuki, E.-i.; Fujii, S.; Fukushima, J.; Takizawa, H.; Wada, Y. Enhancement of fixed-bed flow reactions under microwave irradiation by local heating at the vicinal contact points of catalyst particles. *Sci. Rep.* **2019**, *9* (1), 222.
(241) Torimoto, M.; Murakami, K.; Sekine, Y. Low-Temperature Heterogeneous Catalytic Reaction by Surface Protonics. *Bull. Chem. Soc. Jpn.* **2019**, *92* (10), 1785−1792.
(242) Manabe, R.; Okada, S.; Inagaki, R.; Oshima, K.; Ogo, S.; Sekine, Y. Surface Protonics Promotes Catalysis. *Sci. Rep.* **2016**, *6* (1), 38007.
(243) Zhang, J.; Ma, R.; Ham, H.; Shimizu, K.-i.; Furukawa, S. Electroassisted Propane Dehydrogenation at Low Temperatures: Far beyond the Equilibrium Limitation. *JACS Au* **2021**, *1* (10), 1688−1693.
(244) Zhang, J.; Nakaya, Y.; Shimizu, K. i.; Furukawa, S. Surface engineering of titania boosts electroassisted propane dehydrogenation at low temperature. *Angew. Chem., Int. Ed.* **2023**, *62* (18), No. e202300744.
(245) Corma, A. Heterogeneous Catalysis: Understanding for Designing, and Designing for Applications. *Angew. Chem., Int. Ed.* **2016**, *55* (21), 6112−6113.
(246) Liu, L.; Liu, A. Catalysis paves the way to a new era of the petrochemical industry. *Chem.* **2024**, *10* (4), 1031−1037.
(247) Liu, L. Multiscale structural characterization of shaped catalysts. *Trends in Chemistry* **2021**, *3* (11), 898−901.
(248) Wan, H.; Gong, N.; Liu, L. Solid catalysts for the dehydrogenation of long-chain alkanes: lessons from the dehydrogenation of light alkanes and homogeneous molecular catalysis. *Science China Chemistry* **2022**, *65* (11), 2163−2176.
(249) Huang, M.; Hu, X.; Chen, D.; Maeno, Z.; Tsunoji, N.; Toyao, T.; Shimizu, K.-i. Anaerobic Ammodehydrogenation of Ethane to Acetonitrile over Ga-Loaded H-FER Zeolite Catalysts. *ACS Catal.* **2024**, *14* (2), 1013−1020.
(250) Chen, G.; Fang, L.; Li, T.; Xiang, Y. Ultralow-Loading Pt/Zn Hybrid Cluster in Zeolite HZSM-5 for Efficient Dehydroaromatization. *J. Am. Chem. Soc.* **2022**, *144* (26), 11831−11839.

https://doi.org/10.1021/jacsau.4c00730
JACS Au 2024, 4, 4084−4109